Minimally invasive evaluation of head and neck squamous cell carcinoma

Mark. G. Torchia, MS
Department Human Anatomy and Cell Sciences
and Department of Surgery
University of Manitoba
December 21, 2000.

This thesis is submitted in partial fulfillment of the Doctoral Program.

Table of Contents

Table of Figures

Table of Figures (continued)

Acknowledgments

There is one author on this document's cover, but research is always a team effort. Thank you Cancer Care Manitoba (Surgical Oncology), especially Jenny, Bobbie, and Erin for assistance (and patience!), Drs. Paul Kerr and Donna Sutherland for access to clinics, Corrine Leblanc for MRI wizardry, Dr. Lawrence Ryner for help with Boards and computers, Dr.Steven Ahing for things histological (and wonderful jokes), Dr.Scott Sutherland for radiology advice, and Dr. Randy Aitken, skilled veterinarian, and comrade. My gratitude to Dr. Gordon Grahame, my honorary advisor, whose ethics, dedicated care for patients, and thoughtful discussions kept the real goal in focus. Special thanks to my advisors: Dr. Richard Nason; who launched me into surgical oncology and ran interference in all matters clinical, Dr. Rudy Danzinger; whose advocacy made this possible and from whom I have learned so much, Dr. James Thliveris; who made an sometimes frustrating experience into something rewarding and allowed me the freedom to develop; whose enthusiasm carried me forward. My dear family, last in the text, first in my world; Barbara, Muriel, Erik, you put up with so much. Thank you, thank you. Your quiet concern and continued love made everything possible - each of you deserves a doctorate. [The following provided operational or financial* support: St. Boniface General Hospital Research Center and Foundation, Berlex Canada*, Advanced Magnetics Ltd.*, the Institute for Biodiagnostics, and the University of Manitoba, Department of Surgery.]

This work is dedicated to all the patients that volunteered to participate in this study. You are true pioneers in the improvement of care for all cancer patients.

Abstract

Head and neck cancer represent about 7% of all malignancies in North America, the majority of these tumors being squamous cell carcinomas (SCC) which metastasize to local and regional lymph nodes. In Manitoba, they cause over 70 deaths each year. The goal of the present study was to investigate and develop novel minimally invasive techniques that could allow enhanced evaluation and treatment of patients with head and neck SCC. Human and animal experiments in this study included measurements of tumor microvascularization using dynamic contrast enhanced (DCE) and tumor oxygenation using blood oxygen level dependent (BOLD) and compared them to tumor histology. The detection and identification of sentinel lymph nodes was also investigated. VX-2 tumors in rabbits demonstrated applicability of the DCE and BOLD techniques to a model of SCC. VX-2 tumors showed reduced contrast uptake and decreased oxygenation during development of central necrosis. In patients with SCC, size distribution of microvasculature was shown to be related to tumor recurrence and survival. DCE functions were related to microvessel size distribution, tumor size, and nodal status while BOLD oxygenation studies correlated with tumor microvasculature. Positive nodal status was correlated with a widened oxygenation distribution in the tumors. An MRI based interstitial lymphangiography (MRIL) method using a USPIO contrast agent was developed and proved comparable to the isosulfan blue method. MRIL provides significantly improved anatomic information compared to current sentinel node techniques. Overall, these minimally invasive techniques showed significant promise for enhancing the treatment of patients with head and neck squamous cell carcinoma.

Introduction

Head and neck cancer represent about 7% of all malignancies in North America (1). The most frequent tumour type is the squamous cell carcinoma, followed by adenocarcinoma (primarily in the thyroid and salivary glands), lymphoma, and a number of less common types, including carcinoma (not otherwise specified) and verrucous cancer. Over 75% of the tumors are seen in patients over the age of 50 years although their frequency appears to be increasing in specific subgroups, for instance in younger males in eastern Europe. These tumors show a male to female ratio of 1.5:1 (1). In Manitoba approximately 215 new oral and laryngeal tumors are seen each year with 70 associated deaths. The incidence and mortality in Manitoba have dropped approximately 2% since 1988 (2). Smoking and alcohol are major risk factors associated with oral cancer and are the suggested etiology in over 75% of the cases in North America. Dietary factors and human papillomavirus have also been suggested as causative agents (3). About 5% of the tumors are histologically undifferentiated, 45% moderately differentiated, and the remainder divided between well and poorly differentiated (1). As a rule, these tumors spread by local invasion and metastasize to regional lymph nodes but spread to bone and/or lung can also occur. However, in all cases, tumors that are associated with metastatic lymph nodes have a much poorer prognosis where, for example in tumors of the base of tongue, 5-year survival drops from 53% to 34% with just a single positive node detected (4). The annual risk of these patients developing a second primary tumor is high at 4% and this is thought to be a result of the entire upper respiratory tract being exposed to the same

carcinogenic environment. The overall 5 year survival rate from tumors of the oral cavity and pharynx has remained at approximately 50% since 1974 (5) and for laryngeal tumors the survival has been somewhat higher at 68% but has also remained unchanged (5).

Tumors of the head and neck may present with a variety of symptoms including swelling in the neck, dysphagia, odynophagia, bleeding, hoarseness, otalgia, or nerve deficits (6). In many cases, symptoms do not appear until the tumor is quite large, especially those located in the nasopharynx. In some instances, the only symptom may be an enlarged lymph node in the neck. Investigations include complete history and physical exam. Examination of the oral cavity is performed as well as visualization of the upper respiratory system by mirror or endoscope. Careful attention is made to detection of any enlarged lymph nodes. Biopsy, often using fine needle aspiration techniques, of the primary tumor and/or lymph node(s) is performed early to establish definitive diagnosis. Radiological examination to determine tumor extent and nodal involvement is usually made by computerized tomography (CT) and in some cases magnetic resonance imaging (MRI). In many cases there is good correlation between pathology and radiology, especially in regards to tumor extent, nodal status, and bone involvement (7). The American Joint Committee on Cancer (AJCC) TNM (tumor, node, metastasis) classification (originally proposed by Denoix and Schwartz (8)) is applied to these tumors as a means of staging (progression from stage O for a carcinoma *in situ* to stage IV) for prognosis and treatment (9,10). TNM classifications are occasionally reevaluated based on current survival information. The T portion of the staging system varies considerably

from site to site, whereas except for thyroid cancers, N staging is the same. Distant metastasis is always associated with stage IV disease. Sites of regional lymph node involvement are categorized into anatomic subsites, Levels I through VII, representing submental/submandibular, upper, mid-, and lower jugular, posterior triangle (also referred to as spinal accessory), prelaryngeal and pre- and paratracheal, and upper mediastinal respectively.

Treatment of these tumors is dependent upon the location and stage of the tumors as well as coexisting patient conditions. When treatment is possible the modalities used are surgery, radiotherapy, and chemotherapy. Depending on the situation, these treatments may be used alone or in a variety of combinations. The use of surgery as a single modality ranges from a low of 6% in nasopharyngeal cancer to a high of 85% in cancer of the lip (1). For cure, surgery is based on the complete excision of the tumor with a margin of healthy tissue, typically >2 cm. In many cases this margin is impossible to achieve because of close boundaries to major vessels, nerves, skull base, or bone. In cases where there is obvious nodal involvement, or sufficient reason to suggest that occult metastatic nodes may exist, surgery can include dissection of nodes in the neck. In many centers, standard therapy has involved elective total neck dissection (levels I-V) in patients with positive lymph nodes and in N0 patients where there was a significant chance of occult metastasis (11).With advances in radiological imaging, elective total neck dissection inpatients with N0 necks has been questioned (12,13). Depending on the extent of resection required, surgery can result in some cosmetic disfigurement, especially if

complete neck dissection or mandibular resection is required, or physiologic impairment, including the loss of speech or control over swallowing. Permanent tracheostomy may be required in some cases.

Radiotherapy can be an effective primary treatment for head and neck tumors and is used as a single modality in approximately 30% of tumors of the oral cavity, pharynx, and larynx (1). Lymphomas and squamous cell carcinomas of the nasopharynx and tonsil are particularly sensitive to radiotherapy. The mode of action of radiotherapy is based mainly on the ionizing radiation forming reactive molecules, especially oxygen free radicals, in the tissue and their subsequent effect on cell physiology and activity in the nucleus. Treatment modes include external beam therapy or implantable sources (brachytherapy). Brachytherapy has the advantage of delivering higher doses to more localized areas however external beam therapy remains the mainstay technique. Curative treatment typically requires radiation doses of 6000-7500 cGy. Doses higher than this can result in significant damage to surrounding tissue (14). The dose applied may be less in situations where the radiation field includes radiosensitive structures such as the eyes and spinal cord. The total amount of radiation is administered over the course of 5-8 weeks. Hyperfractionation, where two times daily doses are given has been introduced into some treatment protocols. Lead shielding and multiple field set-ups provide enhanced control over anatomic distribution of the radiation. Neck lymph node metastases are treated simultaneous with the tumor if they can be easily included in the primary field of treatment, or are treated in a separate field. Often, radiotherapy is used as an adjunct

following surgery, especially in cases where a sufficient healthy margin of tissue can not be resected. Radiation can also often used as salvage therapy in patients with recurrence after primary surgical resection.

Chemotherapy has seen a lesser role in treatment of patients with head and neck tumors with approximately 5% of patients treated with this regimen as primary therapy (1). It has not achieved status as a primary curative treatment modality but it can be used to advantage as an adjuvant treatment (15). In tumors of the hypopharynx, where preservation of speech is a primary goal, chemotherapy is been used under protocol in combination with radiation therapy. Primarily, chemotherapy plays an adjunctive role as a radiosensitizing agent, in surgery for tumor debulking, in salvage therapy, and in patients with metastatic disease (14). Immunotherapy is only just beginning to be evaluated in head and neck cancer patients (16).

Patients with extensive tumors are most often not curable and each of the treatment modalities become palliative. Recurrence at the primary tumor site or in neck nodes, ipsilateral or contralateral is not uncommon. Depending on the original treatment, secondary curative treatment can be attempted although in most cases this treatment is not curative. Radiotherapy is one of the limiting factors in treating recurrences since no further radiation can be provided without causing significant local deleterious effects once the maximum curative radiation dose has been given (6).

Measuring treatment effectiveness is limited to histologic examination of the surgical specimen to determine the status of the surgical margin, follow-up clinical examinations, radiological evaluation of the neck, and in the case of monitoring radiation or chemotherapy, radiological evaluation of tumor size and consistency and additional biopsy. Single photon emmission computerized tomography (SPECT) using ^{201}Tl has been investigated as method of monitoring tumor regression but depending on tumor location and size, there may be significant interference from Tl uptake in the thyroid or salivary glands (17). There are no clinically applied techniques available for monitoring progression of treatment that depend on specific physiologic criteria such as reduction of tumor microvascularity or tumor hypoxia as might be seen in radiation therapy or treatment with antiangiogenic compounds.

Treatment regimens for head and neck cancer patients are currently based on clinical and histologic findings including tumor location, tumor size, nodal status, distant metastasis, tumor type and tumor grade as well as local experience of the physicians. Despite the use of these predictive criteria many tumors progress outside the expected nature for their Stage. It is thought that most often this is a result of understaging due to occult lymph node metastasis but may also reflect factors of tumor biology that can not as yet be measured (13,18,19).

Additional tools have been investigated for use as predictive tests to enhance treatment of head and neck tumors. A majority of investigations have encompassed a measurement of

angiogenesis or microvascular density in the tumor. Angiogenesis, or the formation of new blood vessels, is a complex process but is being actively studied, especially within the framework of tumor biology. Judah Folkman (20) published the first paper suggesting that angiogenesis is a significant factor in tumor growth and since that time many other groups have investigated this process, and confirmed its importance in arthritis, duodenal ulcers, and psoriasis (21). Several review papers are available on this subject (22-24). As tumors grow beyond approximately 3 mm in diameter, diffusion can not provide sufficient gas and nutrient exchange to maintain cell viability and it appears that low oxygen tension is one of the precipitating events in the production of vascular endothelial growth factor (VEGF), one of the primary triggers for angiogenesis(25, 26). It has been hypothesized that tumors with a high rate of angiogenesis and therefore well developed microvasculature, would have enhanced growth and metastatic potential (26). Studies of tumors in breast(27-30), lung (31), cervix(32-34), rectum (35), and skin (36) have demonstrated that angiogenesis, measured by either VEGF staining of microvessel density are indicators of malignancy and may be valuable prognostic markers of survival. Staining techniques and tumor heterogeneity remain a concern in contradictory studies (37).Tumor angiogenesis has recently become focal point for development of new general tumor treatments based on antiangiogenic compounds(38-42). The measurements of tumor angiogenic potential and microvascularity have been used as markers for patient survival in head and neck tumors (19, 43-46). Most of the studies that have investigated microvessel density followed the method of Weidner (27) for measurement and based on this information, an international standard method has been suggested (47). There has

been no attempt to consider vessel size as a predictor criteria in any of these studies.

Given that these tumors metastasize primarily, and often very early, via the lymphatic system it would seem logical that specific histological or other tests and criteria about lymphatics need to be investigated in these patients. Indeed, Folkman (48) suggests that lymphatic vessels may not even exist in tumors. Immunological stains for lymphatic vessels are available only for tissue prepared by frozen section, not paraffin blocks (49-51).

An ideal marker(s) for tumor behavior should have the following characteristics: 1) assessment of the tumor to determine invasiveness prior to treatment, 2) noninvasive (or minimally invasive), 3) measurement of physiologic parameters of the entire tumor, and 4) demonstrate correlation between treatment and outcomes. Histological markers, by necessity, are most often established using biopsy samples. These samples can be obtained using a number of techniques including fine needle aspiration (FNA) biopsy, where only relatively few cells might be obtained, or with biopsy forceps, where typically only the most external portion of the tumor can be sampled. While 'worst case' tumor criteria can be reported by the pathologist, there is little doubt that, given the heterogeneous nature of most tumors, biopsy samples may not provide a complete picture of the tumor behaviour, especially those at an invading deep margin. Histologic examination of the entire tumor can be completed following surgery, but by this point in time the overall treatment plan has already likely been determined. In patients where

radiotherapy or chemotherapy is planned as the primary treatment, examination of the entire tumor is not possible.

The determination of lymph node status is an important consideration in patients with head and neck tumors and is perhaps the single most important measure of treatment outcome and prognosis. Even with scrupulous clinical examination and the use of modern radiologic techniques, the rate of occult neck metastasis of head and neck squamous cell carcinoma (HNSCC) is over 25% (52,53). In patients with early stage HNSCC and N0 necks there is significant debate over the two main options for neck management (6, 9, 11, 54) elective node dissection, or observation. If the neck is treated after patients develop nodes the question arises as to whether the overall outcome is worse that those treated with elective node dissection, especially since the latter can result in significant morbidity. At present there is no noninvasive means of identifying whether an occult metastasis exists.

A similar conundrum exists with the treatment of node negative breast cancer with elective axillary node dissection, but this issue is currently being addressed with a technique referred to as sentinel node biopsy (SNB.) The development of this technique has been long in development and Krag has published an excellent historical and methodological review of the topic (8.) The theory behind the sentinel node idea is relatively simplistic. During metastasis via lymphatics, the tumor cells reach the first node(s) in the drainage chain and begin to grow there. If the first node(s) could be

specifically identified and evaluated histologically it might thus eliminate the need for examination of all the nodes dissected *en bloc*. It is important to understand that the node most proximal to the tumor may not necessarily be the sentinel node. Since the first report by Cabanas in patients with penile cancer (55), over 250 articles have been published on the use of sentinel node identification and biopsy, the majority of which have been in relation to malignant melanoma. Many reviews of breast cancer results have been published (56-62). More recently, the technique has been extended its use to patients with cervical cancer (66), lung cancer (67), thyroid cancer (68), and very recently, tumors of the head and neck (69-71). Three specific techniques are being investigated and used clinically. The first method relies on the interstitial or peritumoral intraoperative injection of isosulfan blue dye, followed by dissection of the surrounding tissues, following the path of the colored lymphatic channels until the first node with blue coloration is identified. The second method uses a preoperative interstitial injection of a gamma emitting radiolabeled colloid in place of the dye. At the time of surgery, a hand held gamma detector probe is then scanned over the surface of the skin, until an area of maximum gamma irradiation is noted. The node dissection is subsequently carried out over this area. The third method involves the use of a gamma emitting colloid but relies on scintigraphic imaging to initially detect the location of the sentinel node. The various methods can also be used in combination (72). Once the sentinel node(s) has been identified, it is sent for histological evaluation. Since only one or two nodes are typically sent, it is possible for the pathologists to focus their examination on many serial sections of these nodes. Systematic sectioning protocols for sentinel nodes have been developed

(73). Intraoperative pathologic techniques (frozen sectioning and imprint cytology) for examination of sentinel nodes have also been assessed (74).

A number of issues with SNB remain, most notably the relatively significant learning curve to achieve reproducible results. The blue dye can be difficult to follow especially in complex anatomical areas. If dissection is prolonged a second injection of the dye may be needed. The dye stains surrounding tissues as it extravasates and can obscure the surgical field. The radiocolloid gamma probe method can also be problematic when the tumor is in close proximity to the sentinel lymph node due to significant overshadowing of the radiation fields such as in the tumors of the tongue with submandibular sentinel nodes. Discordant results in node mapping occur between the dye and radiocolloid methods (75) and between differing types of radiocolloid (albumin versus sulfur colloid) (76). Scintigraphy studies can determine an approximate location of the sentinel node but achieves poor spatial resolution and little anatomical mapping detail (77-79). This latter technique requires that the patient be examined in the nuclear medicine department before surgery which adds additional complexity to case scheduling.

Many surgeons have voiced concern over the reliability of the SNB technique and its potential for false negatives. Many studies have investigated this issue and a notable one by Turner and coauthors, reports that in a large series of breast patients (n=60) where 1087 nodes were examined histologically, the false negative rate was only 1.7%. It would therefore appear that the concept of a reporter or sentinel node is correct (80). There

remains however two additional issues: 'skip metastases' and the finding of more than a single sentinel node. The term skip metastasis relates to the observations previous to SNB that in some cancer patients, metastases were not found in the nodes closest to the site of the tumor (81). In a case of squamous cell carcinoma of the tongue where the patient has an elective neck dissection, a node in a more distal neck lymph node basin might contain metastatic cells whereas more proximal nodes do not. Histologic studies have demonstrated these skip lesions in approximately 10% of positive necks (82). For SNB the concerns is that perhaps metastases somehow by-pass the first node(s) in the drainage chain and settle in more distal locations. This does not appear to be substantiated by the false negative results form previous studies. The basis for the phenomena of skip node metastasis may well be anatomical variation where the lymphatic vessel draining the tumor site may simply be directly connected to a node quite remote to the primary site. The observation that patients may have more than one sentinel node can result from one of two possible scenarios.

First, it may be that two nodes are anatomically adjacent and although connected in series still appear to the observer, in the case of the dye method, or to the gamma probe in the case of the radiolabeled colloid, that both nodes stained or traced simultaneously. The other possibility is that indeed, two nodes are sentinel nodes because they are in fact connected in parallel to the same primary drainage lymphatic vessel. This is a matter of anatomical development that should not be surprising given the multitude of anatomical variations seen in the vascular systems. SNB is becoming firmly established as one of the

tools for treating breast tumors and malignant melanoma. However, sentinel node evaluation remains a procedure accomplished at the time of surgical treatment. To better formulate a treatment plan, it would be ideal if the SNB theory could be developed into a technique that would allow a minimally invasive presurgical investigation to permit treatment to be tailored to nodal status.

Over the past ten years the role of radiological imaging in head and neck tumors has been evolving with the introduction of newer modalities such as thin section CT and positron emmission tomography (52). Computerized tomography has been utilized for many years in patients with head and neck tumors to detect and describe the primary tumor as well as for assessment of lymph nodes, although in the latter its reliability is best in bulky nodes (83). CT has a disadvantage in head and neck patients given that dental amalgam creates a significant artifact that may interfere with radiologic diagnosis. Positron emmission spectroscopy appears to be a promising technique for detection of tumors in the head and neck(84, 85) and in detection of positive neck nodes (86). However, this technology is expensive, requires considerable infrastructure, and is presently limited to only a few sites. Doppler ultrasound has shown only modest predictive power for head and neck tumors (87-89).

Magnetic resonance imaging has become a popular procedure for the investigation of many lesions, and in some such as brain tumors or joint injury, is considered to be the primary investigational tool. MRI technology is based on the physical principle of nuclear

magnetic resonance and since mid 1970, the equipment and techniques have been highly refined. The basis for the production of images relates primarily to the reaction of protons (hydrogen atoms) when they are exposed to magnetic a field(s) and radiofrequency energy (90). By altering how and when the magnetic field(s) and radiofrequency pulses are turned on and off in combination with significant data processing, subtle differences in tissue properties can be exploited to provide images of high spatial and tissue resolution. Any radiological image requires contrast between adjacent tissues for detection and examination of the tissue or lesion of interest. In a plain radiograph, contrast between bone and soft tissue may be required, in computerized tomography contrast between vasculature and white matter may be desired, and in ultrasound, contrast between cystic and solid tissues may be important. MRI allows building of sequences (the stepwise series of events between magnetic field, radiofrequency pulses, and detection) to provide a variety of contrast ranges depending on the exact requirements of the clinician. These might require contrasting white and grey brain matter, muscle and fat, or hepatoma from liver parenchyma. In general MRI is best used for its ability to resolve soft tissue. MRI also has the ability to distinguish moving fluid and therefore can be used for angiography or for example, to map the movement of bile within the biliary tree (magnetic resonance cholangiopancreatogram- MRCP). In some situations, contrast differences can be enhanced by the use of a contrast agent. These have be used in plain radiography and computerized tomography for many years. MRI contrast agents have been used to provide enhanced detection of vasculature for MR angiography, better joint studies through MR arthrography, and enhanced tumor detection (91-94). Significant post contrast tumor

signal enhancement is often seen in MR. Current contrast agents do not remain in the vascular space; the enhancement phenomenon is a result of the loss of the contrast agent from the blood pool, through the leaky endothelia of the capillaries, into the extracellular space of the lesion or tumor. It has been suggested that by refining MRI techniques, this enhancement has the potential to be used, within certain limitations (95), for non-invasive examination of biochemical and physiological properties of tissue (96).

Traditionally, MRI examination of tumors has relied on a simple off-or-on approach to tumor contrast enhancement. More recently, MRI data has been used to determine the tumor pharmacokinetics of contrast agent based enhancement, using a technique referred to as dynamic contract enhanced (DCE) MRI. In this type of MR study, slice images through the area of interest are obtained in real-time, before, during, and after the intravenous injection of a bolus of contrast agent, usually through the antecubital vein. A plot of the change in contrast (MR signal intensity) of the region of interest (ROI) versus time can then be derived, similar to what would be done in pharmacokinetic study with serum concentrations of a drug, and fitted to a two compartment model(97, 98). In the bolus or first pass method, the initial increase in the contrast (input function, k_{in}, k_{21}, in sec^{-1}) is a measure of the velocity of the transfer of the contrast agent from the intra- to extravascular tumor space and is a function of blood flow and endothelial permeability. The total change in contrast (amplitude, A) indicates the overall fraction of the extravascular extracellular space (EES) in the tumor. The second phase of the curve (the elimination or distribution function in sec^{-1}), which can demonstrate a slow increase, a

plateau, or decreasing contrast enhancement, reflects the elimination of the contrast agent out of the tumor via the lymphatics and by diffusion of contrast back into the blood vessels as the intravascular concentration decreases. Investigations in the use of DCE MRI have included differentiation of enhancing but benign breast lesions from malignancies (99, 100), detection of synovial inflammation, detection of cervical carcinoma recurrence (101), as well as studies of liver (102), lung (103), thyroid (104), and pituitary tumors (105). While the majority of studies have involved the differentiation of benign from malignant tumors, or the differentiation of malignant tumor types a few have also attempted to correlate the DCE parameters to histological stage (106), to microvessel density (107-109) mixed results. Dynamic CT has been investigated as a tool for determining tumor perfusion in HNSCC but the results have not been positive (110). To date this technique has been well established to predict outcome in a group of single malignant tumor types and has never been used in any investigation of head and neck tumors (108.)

Although some indication of blood supply to the tumor can be measured using the DCE MRI methods described above, blood supply can only imply a degree of tumor oxygenation. A valid measure of oxygenation may be a better indicator of neovascularization intention. A number of studies have investigated the oxygen tension of tumors using a biocompatible microprobe that can be transcutaneously inserted into tumors or metastasis (the Eppendorf computerized system, Hamburg, Germany) (111-114). In these studies, the electrode is inserted and slowly advanced or retracted during

collection of oxygen tension levels. A histogram is then produced based on positional oxygen tension levels. Tumors with a higher percentage of hypoxic areas appear to be more resistant to radiotherapy. As a result, many trials of radiotherapy have now included means for increasing the tumor oxygen saturation with some early mixed results. A recent study by Terras (112) has called into question the validity of the robustness of polarograph methods, and determined that overall, tumors do not appear to be oxygenated on a gradient but are much more heterogeneous in oxygenation on a microscopic level. The overlying problem with this method of determining oxygen saturation is its very poor three dimensional spatial resolution and an inability to correlate the hypoxic areas identified to the anatomy of the tumor and surrounding areas except very grossly. Another method for determining oxygen saturation relies on the intravenous administration of an hypoxia marker such as pimonidazole, or EF5 followed by microscopic examination of the stained or fluorescent tissue specimen (115, 116). This method obviously prevents the presurgical estimation of tumor oxygen saturation, unless a biopsy sample is used. However, tumor oxygen saturation heterogeneity would indicate that biopsy sampling could be prone to sampling bias. The comet assay, which uses cell DNA damage measurements as an indication of hypoxia, also requires a tissue sample (117, 118). Melo and coworkers (119) have investigated the use of SPECT combined with ^{99}Tm-labeled 2-nitroimidazole as technique for locating hypoxic cells within a tumor. Initial studies in mice appear promising although imidazoles can only provide a switched mode of hypoxia with no relative oxygenation measures (115).

Blood oxygen level dependent (BOLD) MRI has been the basis by which functional images of the brain have been obtained (120). In these studies, ultrafast scans of the brain are produced before, during, and after specific motor or sensory functions are performed. In carefully controlled trials, it has been shown that BOLD analysis can indicate which areas in the brain are being triggered. BOLD MRI is based on the principle that oxyhemoglobin and deoxyhemoglobin have distinct magnetic properties, namely diamagnetism (no permanent magnetic moment but when placed in a magnetic field have an induced moment) and paramagnetism (inherent weak magnetic dipole moment). During increased requirements for oxygen the amount of deoxyhemoglobin in the capillaries feeding the monitored tissue increase. This results in an MRI artifact of magnetic susceptibility, specifically when using T2* weighted imaging. This change in the contrast resulting from the change from oxy- to deoxyhemoglobin is measured at a number of echo times and a graph can be plotted of the log increase in signal. The slope of the line has been demonstrated to be indicative of relative oxygenation of the tissues while the intercept is related to the number of vessels ROI.

BOLD has recently been utilized to qualitatively measure oxygenation of blood in vessels (121-124), myocardium(125-128) and renal cortex (129), under respiratory and pharmacologic changes. The use of BOLD MR imaging for the determination of tumor oxygenation in patients has not been reported.

The measurement of lymph nodes using MRI images has been investigated for many years and there remains considerable issue with the use of MRI (or CT for that matter) to specifically indicate which nodes may or may not contain metastases unless the nodes are beyond a certain size, if there is extracapsular spread, or if the node contains obvious necrotic areas. In cases where the nodes are not clinically enlarged the predictive rate of MRI has been limited to 40-60% (89).

Recently, new MRI contrast agents have been produced (although none are accepted for human use in North America) and tested in human Phase I and Phase II trials for use as intravenous lymphangiography contrast agents. Typically these agents are composed of nanometer sized iron oxide (Fe_2O_3) particles coated with dextran to reduce the potential for anaphylaxis commonly seen with intravenous injection iron salts. These agents are phagocytosed by macrophages and are pooled by the reticular endothelial system in the liver and in the lymph nodes (130). As a result, lymph nodes can be preferentially contrasted from surrounding tissues. Interstitial lymphography using MR contrast agents has been studied in rats (130), ferrets (131), and rabbits (132) have demonstrated that lymph nodes grossly replaced with tumor have a pattern of reduced contrast uptake while nodes with benign hyperplasia have relatively normal contrast enhancement (131). Micrometastasis could not be detected in these studies. The potential of MR for sentinel node identification in rats was reported by a study from Advanced Magnetics but single time studies could not distinguish multiple sentinel nodes from non-specific nodal

enhancement (133). Clinical use of these agents as IV lymphangiograph has been initiated and related to identification of gross nodal metastasis (134). The use of these agents for routine clinical use has not been pursued (89).

Rationale and Hypotheses

The purpose of the current study was to determine whether magnetic resonance imaging (MRI) has the ability to provide useful information to the clinician, beyond simple anatomic measurements, that could have predictive utility in the determination of tumor treatment and patient prognosis. Three lines of investigation were: 1) dynamic contrast enhanced (DCE) MRI as a measure of tumor microvascularity, 2) blood oxygen level dependent (BOLD) MRI as a measure of tumor oxygenation, and 3) the novel use of an investigational ultrasmall particulate iron oxide (USPIO) contrast agent for the preoperative detection of sentinel nodes. VX-2 tumors in rabbits were used as an initial test of the MRI methods (DCE and BOLD) in squamous cell tumors. These tumors demonstrate contrast enhancement(135), but have not been studied with either DCE or BOLD MRI. Pigs were used as the model for sentinel node studies as the contrast agent is not yet available in North America for use in humans. Pigs are a good experimental model since they have similar head and neck node drainage patterns to humans and have been used for studies of direct femoral lymphangiography studies (136) (137). DCE and BOLD were also used to investigate tumor vessel and tumor oxygenation heterogeneity using individual-pixel time and spatial functions. Archived tissue from patients with HNSCC were examined using the international method (47) and immunostaining to obtain information about microvascular density and vessel size distribution as a comparison to the DCE and BOLD MRI methods.

The specific hypotheses of the current research project were:

1) The rabbit VX-2 squamous cell carcinoma model will demonstrate basic properties of dynamic contrast enhanced and BOLD MR.

2) In patients with HNSCC, tumor microvascular density is a measure of patient outcome, tumor stage, and nodal metastasis.

3) In patients with HNSCC, the distribution of vessel size in a tumor is an independent measure of patient outcome, tumor stage, and nodal metastasis.

4) DCE and BOLD MRI are technically feasible in HNSCC.

5) DCE functions correlate with tumor microvascular density and distribution of vessel size.

6) BOLD measurements of relative tumor oxygenation will be correlated to tumor vascular supply.

7) Since HNSCC tumors display histological heterogeneity, they will demonstrate heterogeneity in both DCE and BOLD analysis.

8) USPIO contrast agent will behave similarly to radiocolloid materials and be able to demonstrate sentinel node identification.

Methods

Histologic measurement of tumor microvascularity

Eighteen random archived tissue samples were obtained from a list of thirty five previous Manitoba Cancer Treatment Foundation patients provided by Dr. R. Nason, Head of Surgical Oncology. These patients had T1 or T2 squamous cell carcinoma of the oral cavity. All clinical information relating to the tumor, patient outcome, or nodal status was not revealed until histological evaluation and analyses were completed.

Archived tissue blocks were selected on the basis of containing the maximum amount of the tumor tissue available with a normal tissue edge. Six micron sections were cut from each block and processed for automated immunohistological staining of CD-34 and H&E staining (negative and positive controls were included with each staining batch.) CD-34 antibody was obtained form Santa Cruz Biotechnology (Santa Cruz, CA). An oral pathologist reviewed each of the sections and demarcated the interface between tumor and normal tissue. Microvessel counts were performed according to international consensus methods(47, 128). Sections were scanned under low power light microscopy and the area of highest immunostaining was noted. This area was reexamined using 100x and 200x power and the fields with the greatest number of were photographed using a digital camera (Sony DXC950, Sony Canada Limited, Toronto) The images were stored as full color TIFF files for counting. Additional photographs were taken of the section at 40x and 400x as reference images to review and confirm the areas chosen and examined.

Vessels counted included any stained endothelial cells or cell clusters separated from surrounding connective tissue or tumor cells (47). The presence of erythrocytes or of a vessel lumen was not required and vessel size (except for vessel with obvious muscular layers) was not an exclusion criterion. The largest dimension of the vessels was determined using a calibrated marker and these were categorized into three levels: <10 μm capillary, 10-25 μm terminal arteriole, and >25 μm arteriole/venule.

Magnetic resonance imaging studies

This portion of the study was approved by the University of Manitoba Committee on the Use of Human Subjects in Research. Approval was also obtained from the National Research Council (NRC) Research Ethics Board since the majority of patients (11/14) were imaged during NRC research scan time. From an initial pool of 130 patients, fourty-five patients were interviewed for participation in the study MRI study. The history and physical data of each of the forty five patients was reviewed and permission obtained from their physician to interview the patient. Specific information as required by the NRC was obtained during the interview, including criteria that might prevent the patients from being studied including previous surgery, history of seizures or allergies, previous injuries from metal foreign objects, claustrophobia, and other disease states which might be exacerbated during the MRI procedure. Informed consent was obtained from patients, which were provided with an anonymous code for MRI study. Of the 45 patients interviewed, eleven patients were scheduled for an MRI examination. In patients with

tumors for whom the surgeon would normally require an MRI examination, only the MRI clinic exclusion criteria were utilized. Images from these latter patients (n=3) were then obtained for research purposes under the Manitoba Personal Health Information Act (PHIA) guidelines. One of the patients refused to participate after the initial scans due to acute and unexpected claustrophobia. This provided a total of 13 patients for MRI data analysis.

MRI examinations were obtained using a General Electric Signa MR/i 1.5T scanner. All patients were placed supine on the table in the magnet bore. Depending on the location of the tumor and the patient's physical characteristics, either a quadrature head coil or a surface neck coil was utilized. Each patient had a 21 gauge intravenous catheter placed in the left antecubital vein. Scout images were obtained based on the findings from either physical examination of the patient or recent CT films. Both T1 and T2 image sets were obtained initially to determine the exact location of the tumor. For BOLD imaging two sets of T2* images were obtained using gradient echo (dual echo) sequences to obtain T2* measurements at echo times of 9 and 27 ms and 18 and 36 ms. A minimum of eight slices were obtained to cover the complete tumor and adjacent normal tissues. Following this, images for DCE were obtained. Eight slices were obtained in the axial plane through the location of the tumor and surrounding healthy tissue. The complete block of slices was obtained every 12 seconds for a total of 45 time slices using a multiplanar FLASH sequence. After the first five time slices, and during continuing imaging, a bolus of Magnevist (gadopentetate dimeglumine, Berlex, Lachine, PQ) was injected through the

antecubital vein at a dose of 0.1 mmol/kg body mass over ten seconds either manually or using a power injector. Images were obtained during and after the bolus injection. A set of postcontrast T1 images were then obtained.

Post Image Processing

Images were transferred to a General Electric Advantage Workstation for mean region of interest (ROI) measures of DCE and BOLD studies, and individual pixel BOLD clustering using the Advantage Workstation image analysis software Functool. An independent workstation was used for the individual pixel DCE clustering measurements using EvIdent (Event IDENTification software, v5.0, Institute for Biodiagnostics, Winnipeg, MB). EvIdent is designed to extract, cluster, and map pixels that follow similar function curves across temporal and spatial axes. For the mean region of interest (ROI) studies, ROI's were based on the clinical report from the CT and MRI as reported by the radiologist. ROI's were selected as: tumor, tumor centre (area that encompasses approximately the central 10% of the tumor pixel count on the largest slice), tumor periphery (area encompassing the outer 10% of the tumor pixel count on the largest slice), tumor invading front (area encompassing the same volume as the tumor periphery ROI but specifically oriented to include only the described leading boundary of the tumor), adjacent tissue (volume equal to that of the tumor centre but placed in nonaffected but similar tissue on the ipsilateral side at a minimum of one centimeter from the contrast determined boundary of the tumor), contralateral normal tissue (encompassing the same

volume as the center of the tumor ROI but on the contralateral nonaffected side), and normal muscle (ROI same volume as tumor centre placed in the left splenius capitis). An additional ROI was placed over the largest artery immediately adjacent to the anatomy of interest. For individual pixel analyses by EvIdent, three ROI's were selected to perform clustering (across the temporal axis), namely the entire slice volume, a volume including the tumor but with a five centimeter boundary of tissue (wherever possible), and a volume including the tumor with a one centimeter boundary. Cluster analysis was performed without filtration of data. Each ROI underwent clustering at two levels; minimum cluster number = 2 and initial cluster number=2, and minimum cluster number=2 and initial cluster number=10, to provide for a coarse and fine cluster amalgamation. Clusters were mapped in colour onto the anatomical MRI images and the images were stored along with their corresponding function curves.

For individual pixel measurements of the BOLD MRI images, the entire MRI slice image was utilized. The images from each dual echo image set were interleaved and bound together using the Advantage software to form a single series with ordered TE times of 9, 18, 27, and 36 msec. Calculation by integration of the maximum slope decrease was then performed using Functool. Thresholding of the images was based on the minimum value that would encompass the entire tumor boundary. Color mapped images representing slope differences were stored as TIFF files. The colour images were converted to 8 bit grey scale maps and the tumor boundary ROI established by overlaying the appropriate anatomical MRI image. The slice containing the maximum tumor volume was always

utilized. Frequency distributions of the tumor grey scale individual pixel images were calculated to provide a measure of tumor T2* (BOLD) heterogeneity.

MRI Parameter Calculations

Three parameters were calculated from the completed DCE curve for each RIO: the input function (slope of the initial rise in MRI signal), the maximum increase in MRI signal (span or amplitude), and the distribution function (slope of the post rise component of the DCE curve). The relative oxygenation from T2* values were calculated according the method of Prasad et al (129), based on the slope of the function from the plot of log-intensity versus echo time.

VX-2 Tumors in Rabbits

Experiments in rabbits were approved by the University of Manitoba Protocol Management Review Committee and all animals were treated according to the guidelines provided under the Canadian Council on Animal Care. VX-2 tumor cells are transformed cells originally from a rabbit squamous cell carcinoma. These cells produce rapidly growing tumors that produce lymph node metastasis in approximately 80% of implants(138, 139). These cells cannot be grown in vitro but must be continued through in vivo implantation, cell harvesting, and freezing for storage. Original cells were obtained from Dr.G.Wolff (Tufts University) and stored at -70C until use. Frozen cells

were rapidly defrosted in warm water and washed and centrifuged (1500g) three time with Hanks buffered saline solution at 4C. Cells were resuspended in RPMI buffer for injection at a concentration of 10^7 cells per milliliter. Cells were used within 30 minutes of preparation.

Eight rabbits (4.5 kg) were food fasted for a minimum of 12 hours and then anaesthetized with isoflurane:O_2 by inhalation to a light surgical plane of anaesthesia. Hair was shaved from the lateral aspect of both thighs and the skin prepared with iodine solution and alcohol, followed by rinsing with sterile saline. The tumor cell suspension (0.5 ml) was injected into the left and right femoralis major muscle at a depth of approximately 1.0 cm using a 1cc syringe with a 25 gauge needle. The full volume of cell suspension was deposited in one location and care was taken to avoid seeding cells along the injection tract. Rabbits then recovered for one hour in an incubator with supplemented oxygen before being returned to their cages. Animals were given free access to water, pelletized food, and occasional fresh vegetables. Daily health checks were performed on the rabbits with particular care given to palpation of the lateral thighs for tumor detection. Tumors were allowed to grow to a maximum of 28 days or to 5 cm in diameter. If it appeared that the tumors were causing pain as detected by change in normal activity or guarding, or if gait was seriously hampered, or if the tumors ulcerated through the skin, the rabbits were anesthetized, studied by MRI, and euthanized. Animals were studied by MRI at days 4, 7, 18, and 28 days using both DCE and BOLD techniques. One rabbit was euthanized and studied on day 27 as a result of necrosis of overlying skin.

Rabbit MRI

MRI examinations in rabbits were performed using the 0.2T Siemens Viva open interventional magnet at St. Boniface General Hospital Research Centre. For study, rabbits were food fasted for 12 hours and then anaesthetized with isoflurane:O_2. Anaesthesia was maintained during the MRI imaging procedures. MRI BOLD images were captured using a dual echo gradient recall echo sequences at echo times of 14, 29, 43, and 57 ms. Five (4 mm) axial slices were obtained with the middle slice centred on the bulk of the tumor. DCE studies were accomplished using a single slice FLASH sequence every 12 seconds over a ten minute period. The slice was chosen to contain the widest area of tumor based on initial T1 images. Following the collection of 5 baseline images, and during continuing imaging, an intravenous bolus of Magnevist contrast agent (gadopentetate dimeglumine, donated by Berlex Canada, Lachine, PQ) (0.1 mmol/kg) was injected by hand over a period of 5 seconds.

Post image processing was accomplished using the Siemens Numeris software (v5.8b) image analysis package. ROI's for both the DCE and BOLD rabbit studies were limited to whole tumor, tumor centre, tumor periphery and normal femoralis muscle.

Rabbit Histology

Rabbits were euthanized by pentobarbital overdose, and each tumor removed *en bloc* from the thigh and fixed in buffered formalin for 24 hours. Following fixation and

dehydration, the tumor was blocked in paraffin and 6 μm sections were cut, mounted on glass slides, and stained with H&E for light microscopy.

Pig Sentinel Nodes

This study was carried out in accordance with the Canadian Council on Animal Care guidelines and was approved by the University of Manitoba Protocol Management and Review Committee. Seven female swine (40-50 kg) were used in the study. Imaging was performed on a Siemens 0.2T Open Viva system and included both spin echo and FLASH 2D sequences in axial and sagittal planes of the head and neck (posterior canthus to the suprasternal notch) and the hind limb (stifle (knee) to the mid-abdomen). An initial 3 pigs were anesthetized using a combination of metatomidine and ketamine and maintained with isoflurane. However, metatomidine appeared to cause respiratory depression and the remainder of the pigs were anaesthetized using only isoflurane to a light surgical plane. All of the pigs were intubated, had a lateral or median auricular vein catheter placed as well as a urinary catheter. A slow saline infusion was maintained for emergency vascular access for sedation of the pigs with diazepam if required. Complete vital signs were taken every 20 minutes and EKG and end tidal CO_2 measured continuously.

Pig MRI Imaging

After obtaining baseline MR images, and during 2 minutes of fluoroscopic mode MR, 0.5 ml of Combidex® (donated by Advanced Magnetic Incorporated, Boston, MA) (either 10 mg/ml Fe or 0.4 mg/ml Fe, randomly assigned) was injected (1.0 cc syringe, 1.5" 23 gauge needle) into the left or right posterior tongue respectively (immediately adjacent to the mandibular third premolar) at a depth of 1 cm and subcutaneously at the right and left stifle (knee) over the tibial tuberosity. Each pig was imaged at 0, 0.5, 1, 2, 4, 6, 24, and 48 hours. Pigs were allowed to recover from anaesthesia with full access to water after the 6 hour and 24 hour image collection.

Pig Isosulfan Blue Dye Sentinel Node Confirmation

During the 48h MRI study, the locations of each of the identified lymph nodes were mapped onto the surface of the pig using the MRI patient table laser cross hair coordinate system matched to the distances on the images. Hard copy film images were also printed for each node location. Immediately following the final imaging, the pigs were taken to the operating room, and a standardized intraoperative sentinel node detection procedure was performed at the same Combidex injection locations in the tongue and hind limb using isosulfan dye (1%, Sigma Chemical Company, Chicago, IL). The right and left sides were completed separately. In the neck, a midline skin incision was made from level of the mentalis to the suprasternal notch to permit rapid visual detection of the dye tracing

and any sentinel nodes. Two milliliters of isosulfan blue was injected into the tongue in the same locations as contrast and the draining lymph vessels identified and their course followed by rapidly dissecting the surrounding tissue in the neck. For the lower limb, 2 mL of isosulfan blue was injected subcutaneously at the stifle but skin dissection (patella to femora vein) was completed two minutes later to prevent disruption of any subcutaneous lymphatic vessels. The first lymph node(s) along the dyed draining vessel were noted for brown (USPIO) and/or blue coloration. Sentinel nodes identified on the MR images were compared and matched to those identified by the dye method. All identified nodes were dissected, fixed in buffered formalin, and processed for light microscopy. Six micron sections were cut and stained using the Perl method for Fe_2O_3. Fresh nodal tissue was also processed for evaluation by electron microscopy.

Statistical Analysis

For comparison of continuous numeric ordinal variables between bilevel groups the Mann-Whitney U test was used and for comparison between three or more groups the Kruskal-Wallis H test was used. Both of these tests are non-parametric tests, the latter being equivalent to a non-parametric ANOVA. Fishers Exact test was used for two by two contingency tables ($n<20$) without ordered variables, Gamma coefficient for 2x2 tables with ordered ordinal variables, and χ^2 for ($n>=20$). Linear relationships were tested by bivariate correlation using the Spearman Coefficient for non-parametric data. Multicategorical variables were modeled using sets of binary comparisons to prevent bias through assumption of linkages between the categorical subgroups. Survival curves were analyzed using the Kaplan and Meier method with comparisons between survival measured using the log-rank test. Some continuous variables were transformed to bilevel ordinal values for analysis by splitting the variables into high and low levels based on the median. Cox Regression was used to model time-to-event data with analysis of multiple covariates as predictor variables. Both Kaplan and Meier and Cox Regression methods allow for censored cases. In all statistical tests, two-tailed significance was achieved at $p<0.05$. Statistics were computed using SPSS for Window, v.10.0 (Chicago, IL.)

Results

Rabbit VX-2 Tumor Models

All rabbits injected with VX-2 cells developed tumors. After approximately 7 days, tumors could be easily palpated as a discrete swelling in the body of the femoralis muscle. MRI imaging could detect tumor growth as early as four days following injection. After the three week period, tumors varied in maximum dimension (approximately 3.0 to 5.0 cm). In one rabbit, skin necrosis over one tumor site occurred at 18 days. At dissection, the tumors were not encapsulated and were well integrated into the surrounding muscular tissue. This was confirmed on microscopic evaluation (Figure 1).

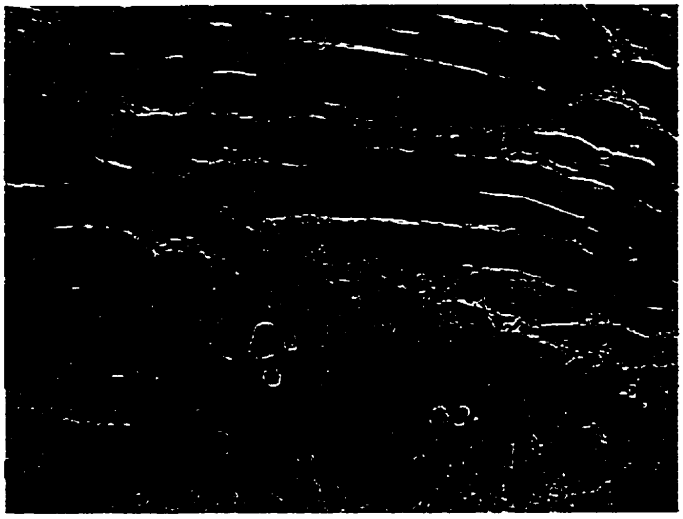

Figure 1 - VX-2 tumor in rabbit showing invasion of surrounding muscle by tumor cells (100x).

Rabbit Dynamic Contrast Enhanced MRI

Dynamic Contrast Enhanced (DCE) MRI of the VX-2 squamous cell carcinoma was successfully achieved in the rabbit. The plot for the main body of the tumor demonstrated an initial rise in contrast followed by a slower decrease in signal (Figure 2.)

Figure 2 - MR signal intensity over time

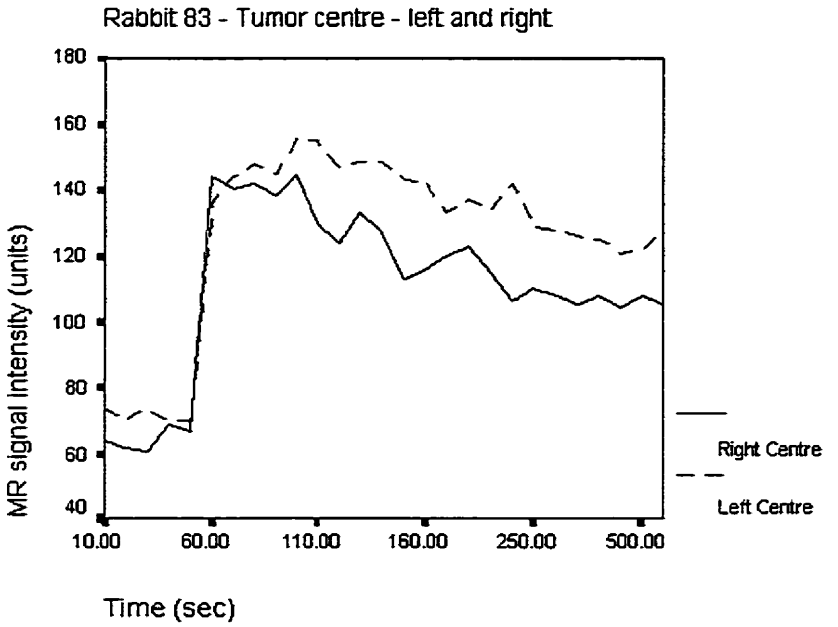

This function was consistent from the time the tumor was visible on T1 weighted MRI until the tumor demonstrated obvious central necrosis on MRI images (Figure 3) (approximately day 18, or 3 cm in diameter.)

Figure 3 - MR image of VX-2 tumor in rabbit thigh showing areas of necrosis (N) within the tumor body (T).

Once loss of viable tissue occurred at the tumor centre, the DCE plot reverted to a non-enhancing pattern (Figure 4.)

Figure 4 - MRI signal intensity over time

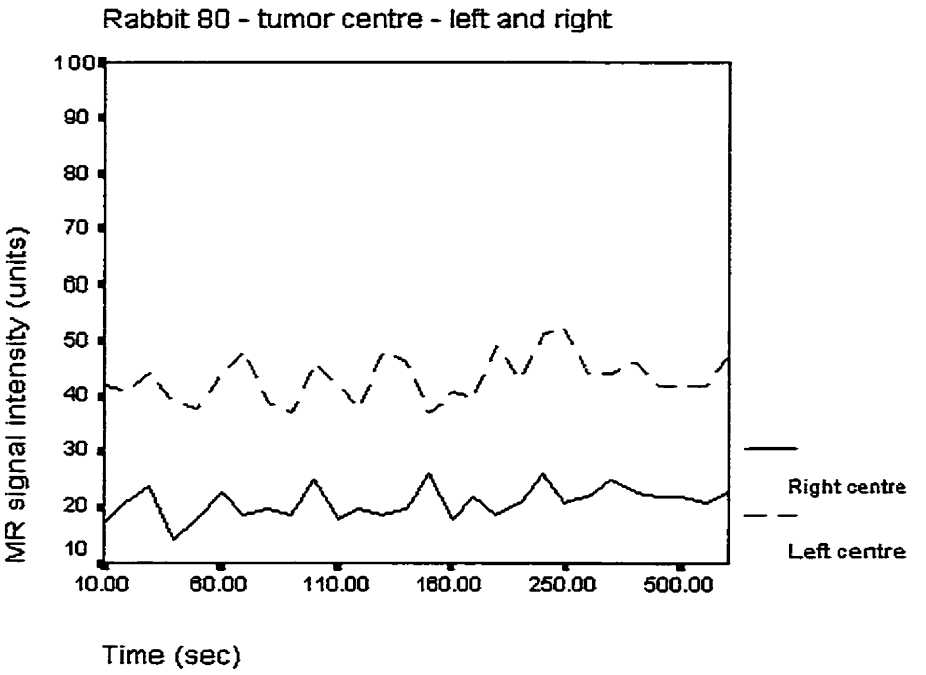

Plots for the region of interest overlying the developing edge of the tumor consistently demonstrated the bifunctional DCE curve (Figure 5) at all times during tumor growth.

Figure 5a - MR signal intensity over time

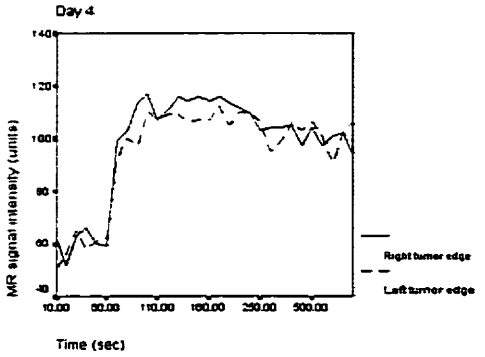

Figure 5b - MR signal intensity over time

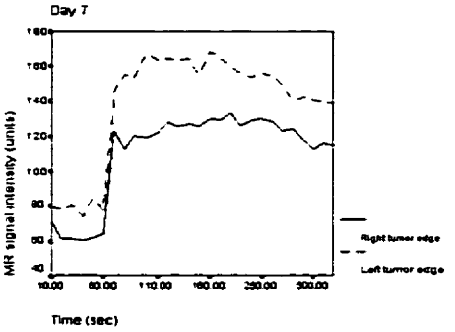

Figure 5c - MR signal intensity over time

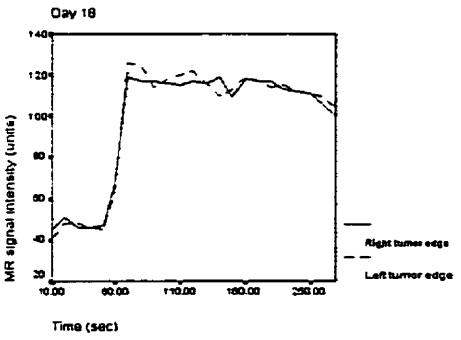

Figure 5d - MR signal intensity over time

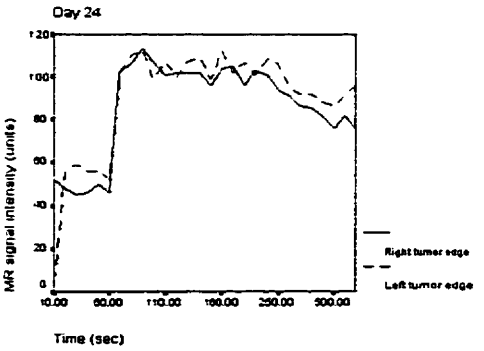

ROI's from adjacent tissue that appeared normal on MRI also demonstrated contrast enhancement to varying degrees although this varied between animals and tumors. There was no obvious enhancement of normal femoralis muscle (Figure 6.)

Fig 6 - Graph of MR signal intensity over time

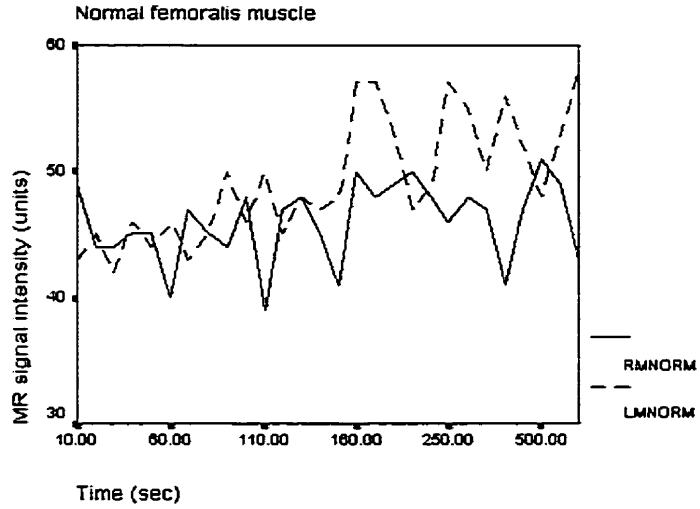

Central portions of the tumor demonstrated a linear relationship of the distribution function over time ($p<0.04$) (Figure 7.)

Figure 7- Plot of DCE distribution slope over time

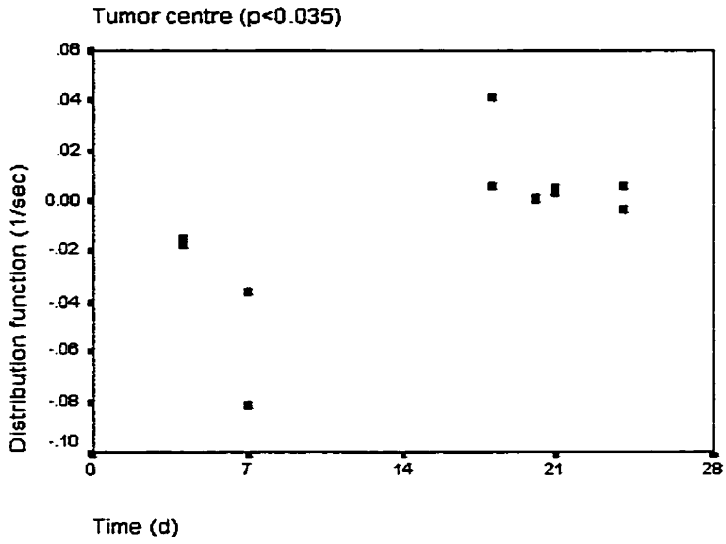

No other trends could be demonstrated. A complete set of rabbit DCE data plots are shown in Appendix A (CD-ROM).

Rabbit Blood Oxygen Level Dependent (BOLD) MRI

BOLD imaging was successfully implemented in the VX-2 squamous cell carcinoma rabbit model. As in the DCE study, BOLD values of the ROI of the tumor centre were reliable until the time that necrosis was obvious on MR images. Relative oxygenation values remained constant in normal rectus muscle and adjacent normal appearing tissue, while oxygenation in the central portions of the tumors decreased over time ($p<0.05$) (Figure 8.)

Figure 8 - Oxygenation of tissue over time

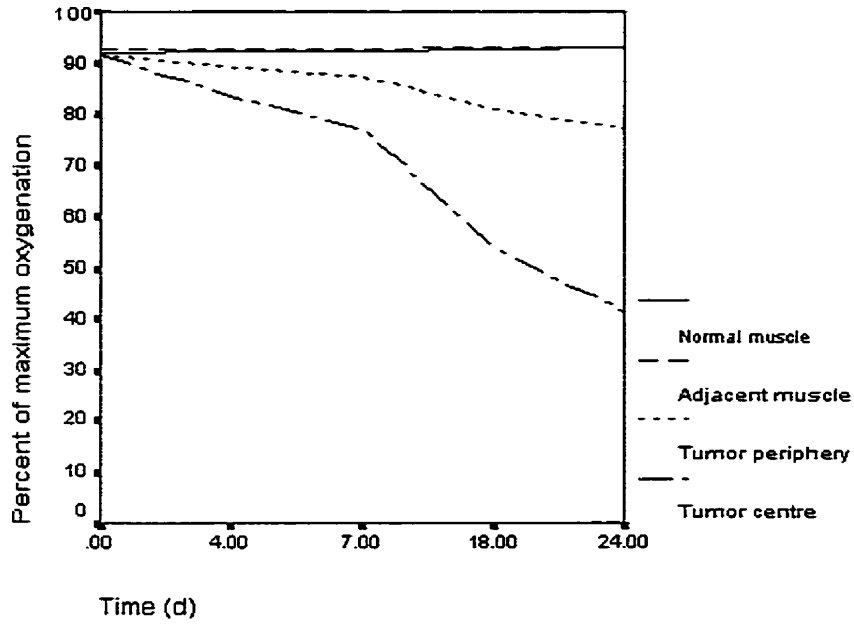

Complete data (T2* slopes) are shown in Appendix B (CD-ROM).

Microvessel Density in HNSCC

CD-34 proved to be reliable immunohistological stain and was used for all measurements of microvascularity. There was a wide range of vessel counts and percentage of the three groups of vessels sizes (Table 1.)

Table 1 - Descriptive statistics of vessels count variables

Variable	Mean	S.E. Mean	Minimum	Maximum
Total number of vessels	23.6	1.8	8	47
Number of vessels <15 μm per HPF	8.1	1.0	0	17
Number of vessels 15-25 μm per HPF	5.8	0.8	1	19
Number of vessels >25 μm per HPF	9.7	1.1	2	21
Percentage of small vessels	34.9	4.4	0	72
Percentage of medium vessels	24.3	2.1	11	50
Percentage of large vessels	40.8	3.7	11	83

Total vessel count and percentage of medium sized vessels were not related to positive node status, node stage, tumor stage or overall staging, recurrence or patient survival. Percentage of large vessels (>25 μm) in a high power field increased with tumor stage ($p<0.05$, Table 2.)

Table 2 - Percentage of large vessels by tumor stage

Stage of Tumor	Mean	S.E. Mean
1	30.5	3.2
2	42.1	6.2
3	52.5	8.4
4	72.1	0.7
Overall	40.8	3.7

Patients with a high percent of smaller vessels (median split) were less likely to have positive nodes at the time of diagnosis ($p<0.05$) (Table 3), while patients with a high percent of large vessels were more likely to have positive nodes at the time of diagnosis ($p<0.03$)(Table 4).

Table 3 - Low and high percent of small vessels by node status at diagnosis

Node / Small Vessel %	Negative	Positive
LOW	8	9
HIGH	9	5

Table 4 - Low and high percent of large vessels by node status at diagnosis

Node / Large Vessel %	Negative	Positive
LOW	10	6
HIGH	7	8

Higher large vessel percentage was also associated with increasing overall tumor stage ($p<0.05$ Table 5).

Table 5 - Low and high percent of large vessels by tumor stage

Large Vessel % \ Stage	1	2	3	4
LOW	8	7	0	1
HIGH	1	7	2	5

Patients with high percent of small vessels in their tumors had a longer time to recurrence (4.7 yrs versus 1.0 years, $p<0.002$, Figure 9) and an increased overall survival (90 months versus 12 months, $p<0.001$, Figure 10).

Figure 9 - Recurrence by %small vessels

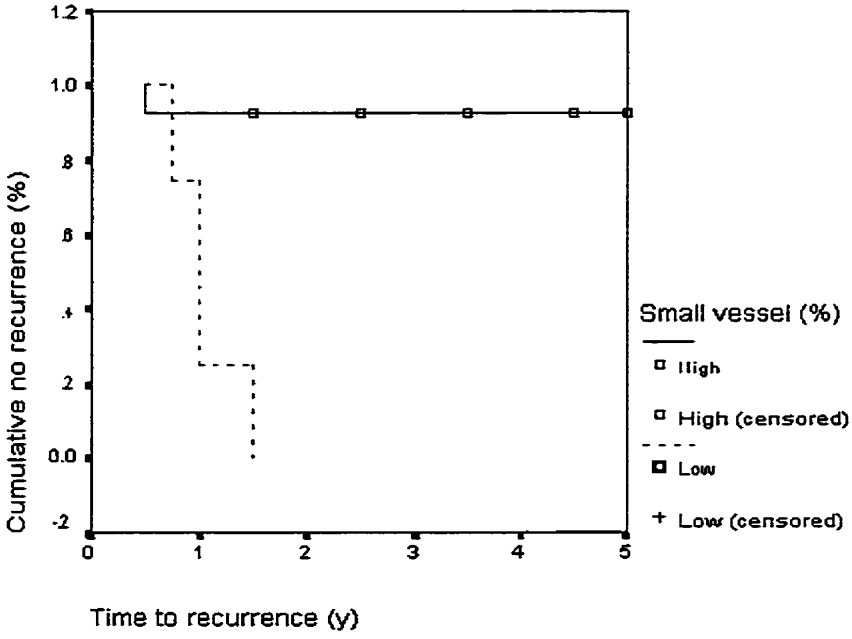

Figure 10 - Death from original disease

by %small vessels

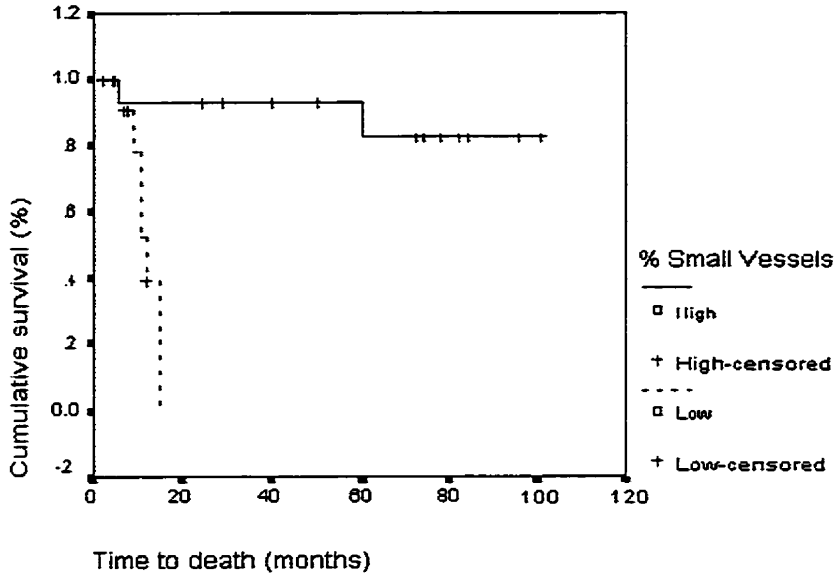

There was no difference in survival in patients who had positive nodes at the time of presentation compared to node negative patients. Cox-regression testing demonstrated that the percent of small vessels (high-low based on median) was an independent (and the only) predictor of patient survival. Complete data for vessel counts can be found in Appendix C (CD-ROM).

Dynamic Contrast Enhanced (DCE) MRI in patients with HNSCC by ROI Average

DCE was successfully completed in 12 of the 13 patients that completed MRI. The single case of unsuccessful MRI was caused by an incomplete injection of contrast agent due to

leakage at the connection between the power injector and the antecubital intravenous line. In the remainder of patients, all DCE examinations results in temporal plots that followed the expected two phase curve (Figure 11.)

Figure 11 - Dynamic contrast enhanced MRI

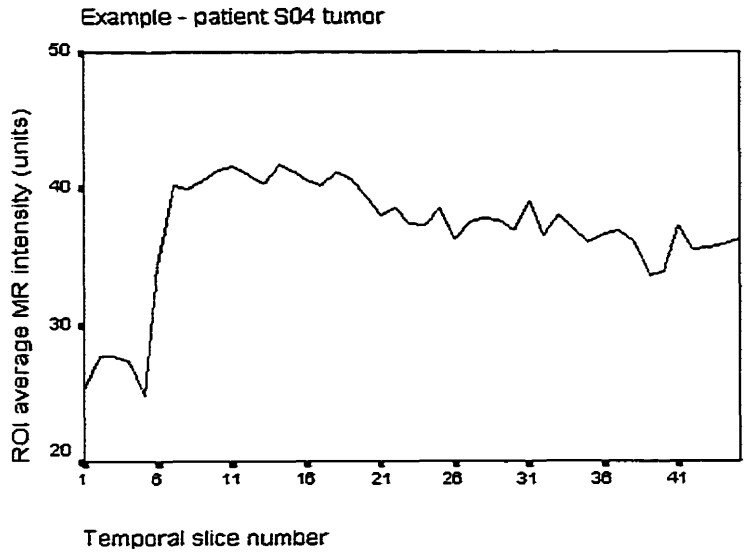

There were graphical differences between DCE curves for each patient, and for each area of the tumor, normal tissue, and blood vessel for a single patient. Tumor ROI's had larger input function slopes, larger total contrast enhancement, and larger negative distribution function slopes ($p<0.05$) than ROI's in normal adjacent tissue, contralateral normal tissue, and normal muscle (Table 6).

Table 6 - DCE factors by tissue location

Location	Input Function (sec^{-1}) (Mean±S.E.)	Span (MR Units) (Mean±S.E.)	Distribution Function (sec^{-1}) (Mean±S.E.)
Tumor	0.58 ± 0.53	18.3 ± 12	-0.0012 ± 0.00016
Adjacent Normal	0.22 ± 0.10	9.8 ± 6.6	*0.001 ± 0.02
Contralateral Normal	0.22 ± 0.17	10.0 ± 4.7	*0.004 ± 0.03
Normal Muscle	0.16 ± 0.01	6.0 ± 3.5	*0.004 ± 0.01

There was no difference in input function slope, total contrast enhancement, or distribution function slopes between the ROI's in tumor, tumor centre, or tumor invasive front. Total increase of enhancement linearly related to the tumor size ($p<0.028$, Figure 12)

Figure 12 - Span of MR intensity change by tumor maximum diameter

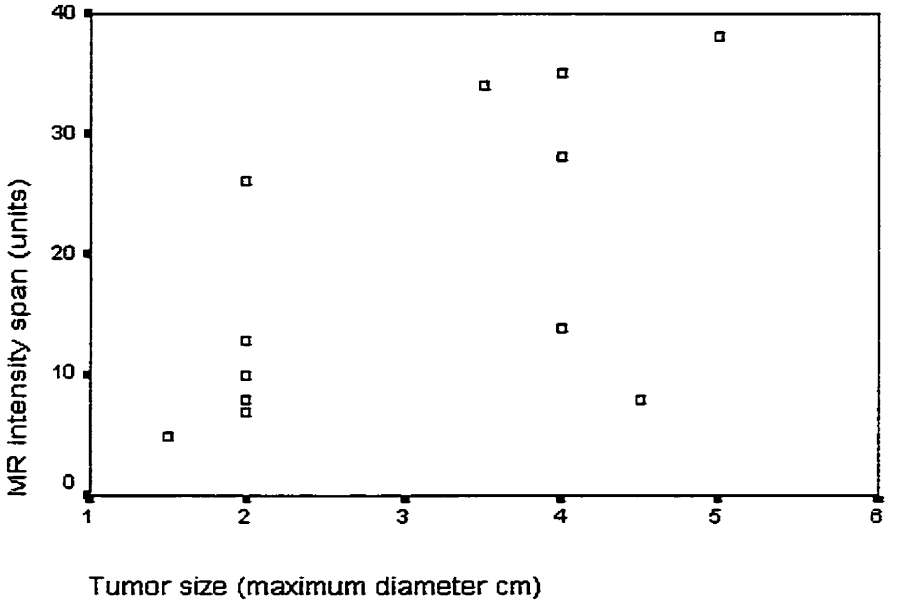

The distribution function of the tumor ROI was correlated with the number of large vessels (>25 μm) per HPF ($p<0.05$, Figure 13). There was no relationships between the DCE input function and nodal status, tumor stage, or vessel count parameters. Complete data can be found in Appendix D (CD-ROM).

Figure 13 - DCE Distribution function versus number of vessels >25 um

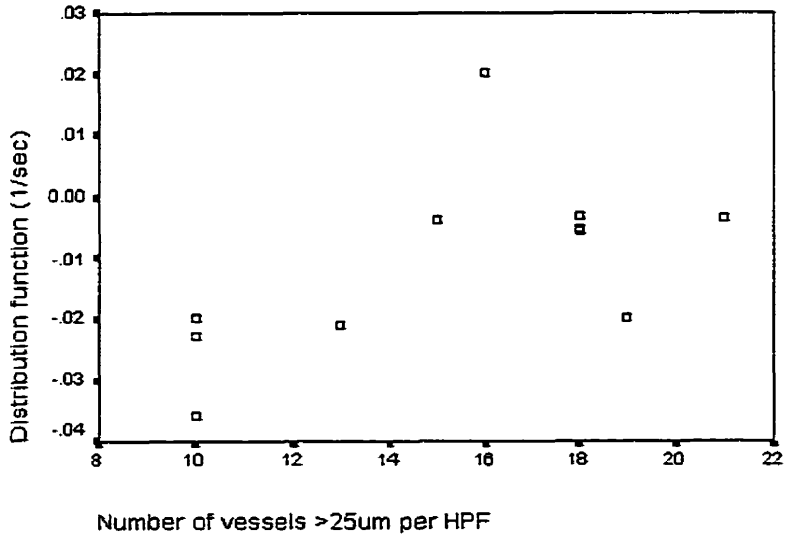

Dynamic Contrast Enhanced (DCE) MRI in patients with HNSCC by Pixel Analysis

EvIdent clustering demonstrated that each of the tumors had numerous sub-populations of pixels that could be clustered by the shape of the DCE curve specific to that sub-population. The individual clusters could then be mapped onto the anatomic MRI images. Figure 14 shows a set of pixel clusters for patient S04 with their corresponding DCE curves.

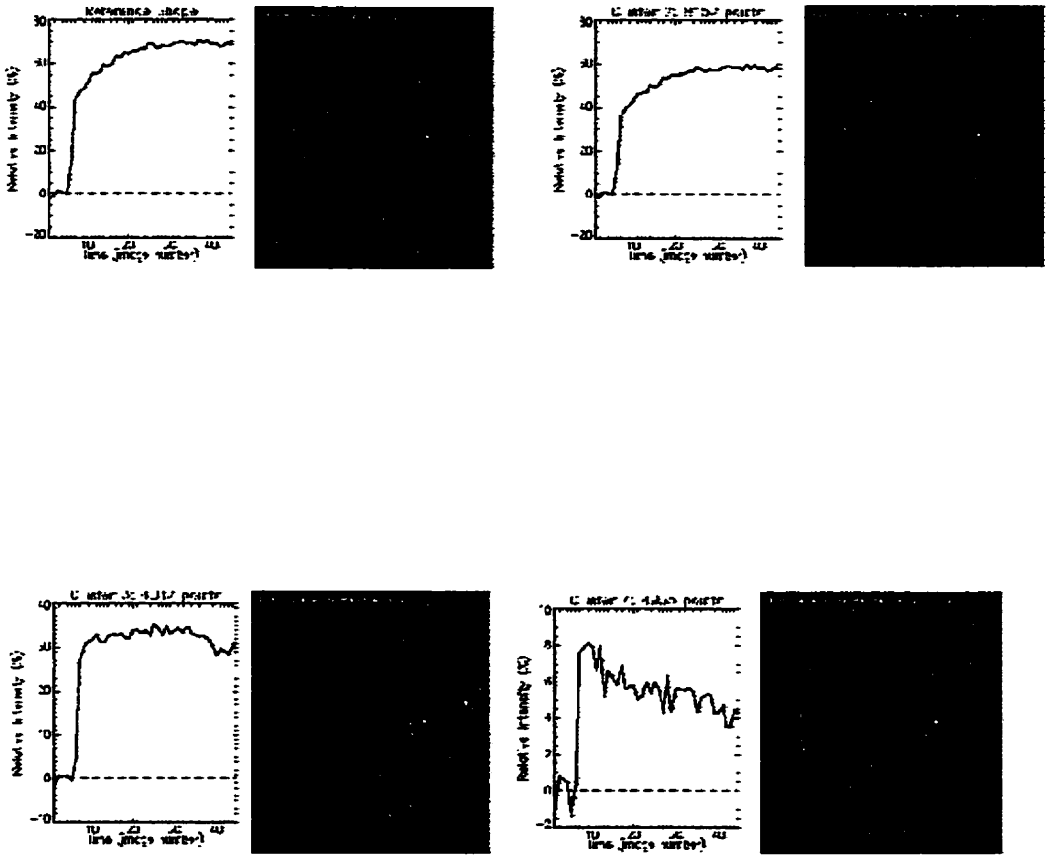

Figure 14 - Example of EvIdent clustering analysis of Patient S04

Each patient's tumor demonstrated varying numbers of and shapes of clustered DCE curves. DCE curves varied widely in their input function slopes, total intensity change, and distribution function slopes. In many patients, specific pixel sub-populations identified specific anatomical features of the tumor, for example a rim of enhancement (Figure 15), main tumor body (Figure 16), or presumed healthy tissue surrounding the tumor (Figure 17). In other cases, the clusters were limited to small fields internal to the tumor itself (Figure 18.) No statistical analysis was performed on these results because of the wide inter- and intra-patient variability The complete set of EvIdent analyzed MRI

DCE images are found in Appendix E (CD-ROM).

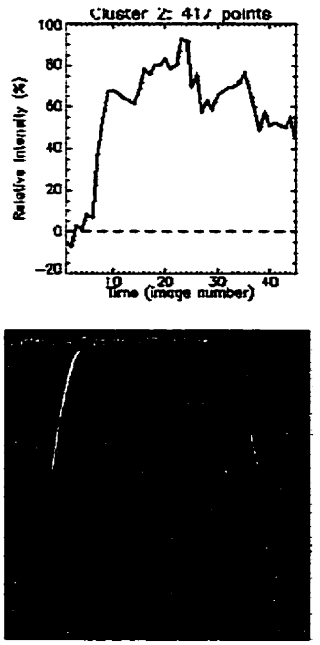

Figure 15 - Cluster analysis of patient S05 showing tumor rim.

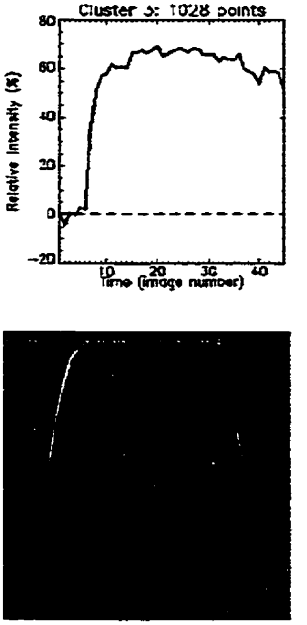

Figure 16 - Cluster analysis of patient S05 showing main tumor body.

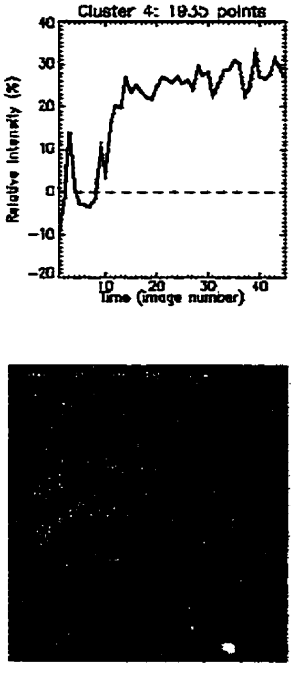

Figure 17 - Cluster analysis of patient S02 showing normal tissue

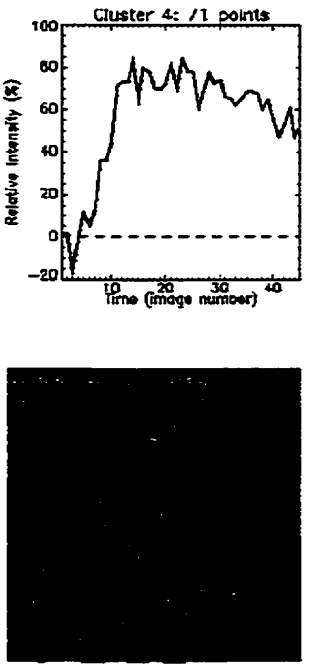

Figure 18 - Cluster analysis of patient S02 showing intratumor clusters.

Blood Oxygen Level Dependent (BOLD) MR Imaging by ROI Average

BOLD analysis was successfully completed in 11 of the 13 patients undergoing MRI. Two of the patients undergoing MRI for clinical purposes did not have BOLD analysis due to examination time constraints. The BOLD analysis data for one patient was lost due to corruption of the magneto-optical storage disk. Tissue relative oxygenation levels varied between patients for all tissues ROI's; values for the tumor are shown in Figure 19. For any one patient (Figure 20), oxygenation levels also varied between tissue types. The complete data set for BOLD values can be found in Appendix F.

Figure 19 - T2* slopes of tumor ROI

for five individual patients

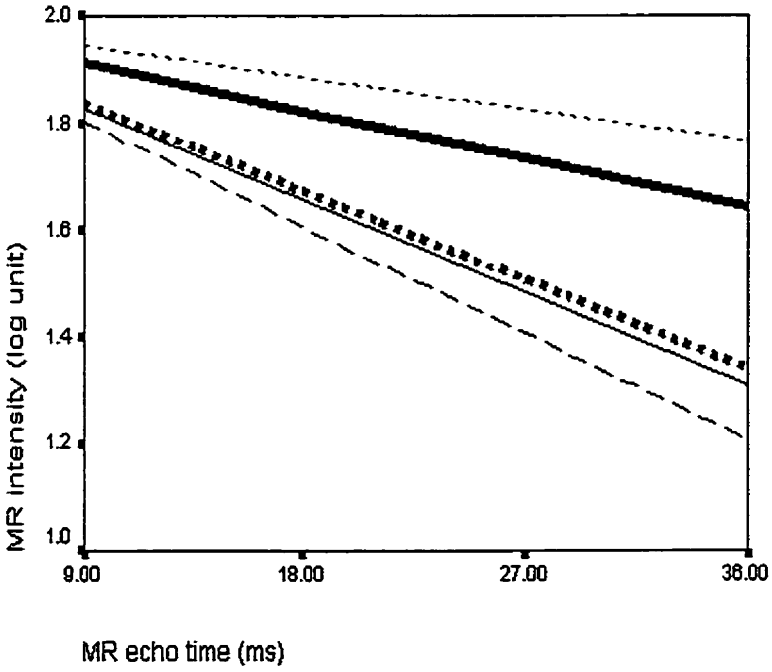

Figure 20 - T2* slopes of for patient S04

by location of ROI

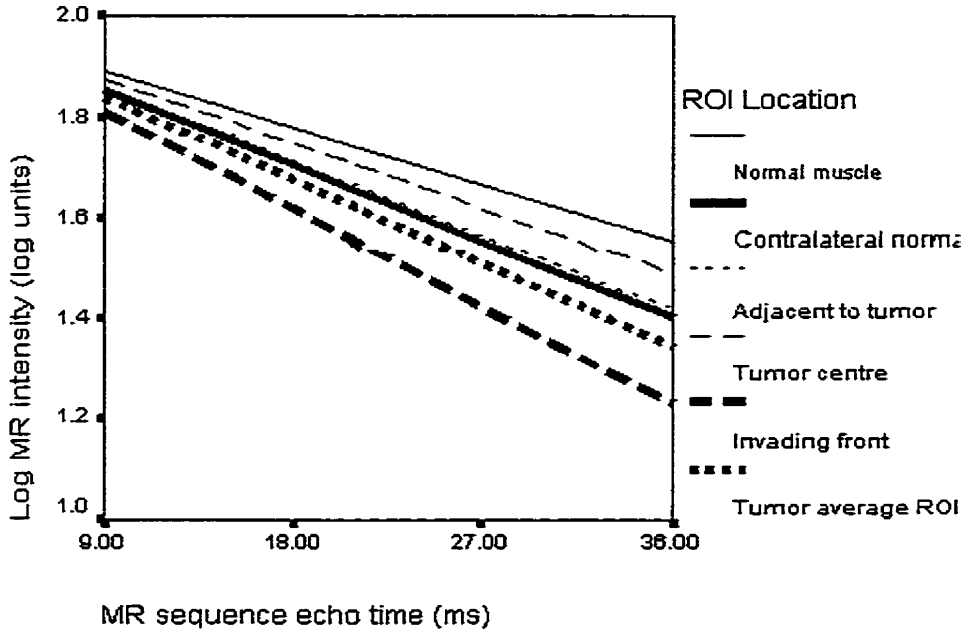

Slope of the T2* lines for the ROI representing the average relative tumor oxygenation were correlated with tumor size ($p<0.02$, Figure 21) where the largest tumors demonstrated the highest oxygenation, but slopes were not correlated with overall stage.

Figure 21 - Slope of T2* by tumor size

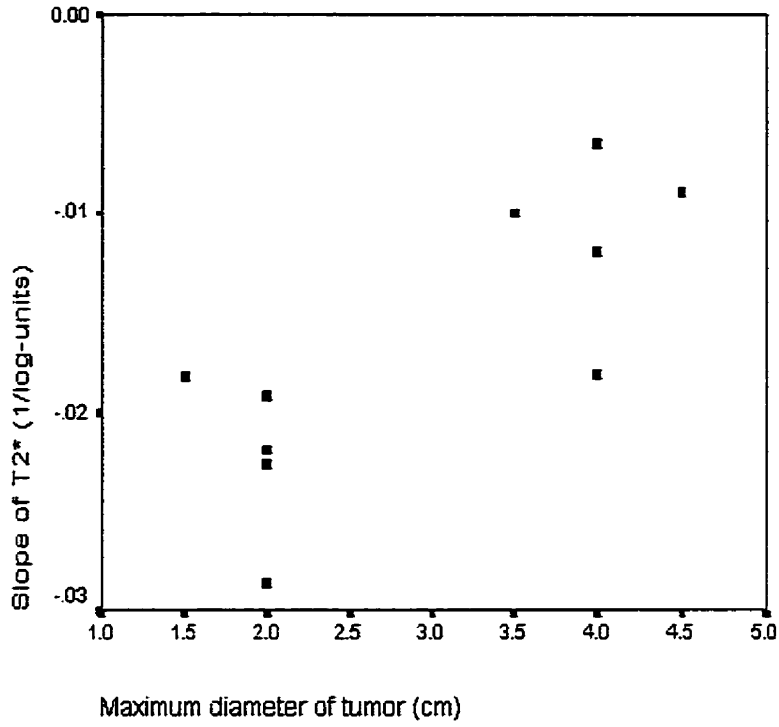

The intercept of the T2* plots did not correlate with any patient or tumor parameters. Patient hematocrit values (at time of presentation) were inversely correlated with stage ($p<0.002$) and tumor size ($p<0.03$.) Lower hematocrit values were also seen in patients with positive nodes ($p<0.05$).

Blood Oxygen Level Dependent (BOLD) MR Imaging by Pixel Analysis

Pixel analysis based on the integral of negative enhancement identified two groups of patients, those with tumors that had relatively consistent T2* values (oxygenation) (narrow distributions) (Figure 22) and those with tumors that had many differing T2* values within the tumor (wide distribution)(Figure 23.) Analysis of the data based on narrow versus wide distributions of T2* values within the tumor ROI demonstrated that wider distributions were associated with lower T2* slopes ($p<0.01$) (increased oxygenation), higher DCE input function (log function, $p<0.02$)), and decreased serum Hgb and Hct levels ($p<0.01$)(Table 7.) Wide T2* distributions were associated with positive nodes ($p<0.01$)(Table 8) and tumor stage ($p<0.01$)(Table 9). A complete set of BOLD distribution photographs and plots can be found in Appendix G.

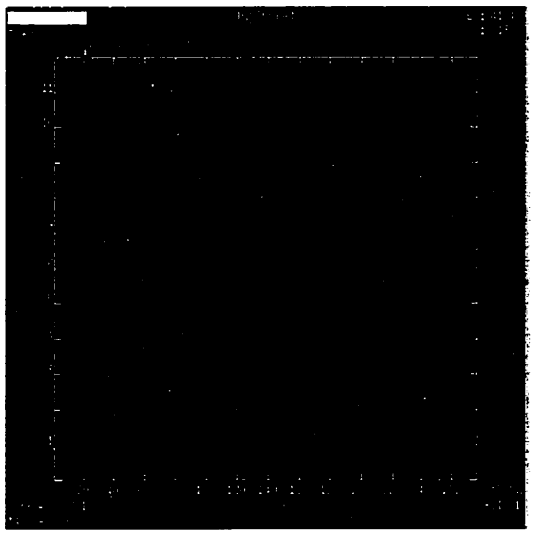

Figure 22 - Distribution of T2* slopes by pixel (Patient S011)

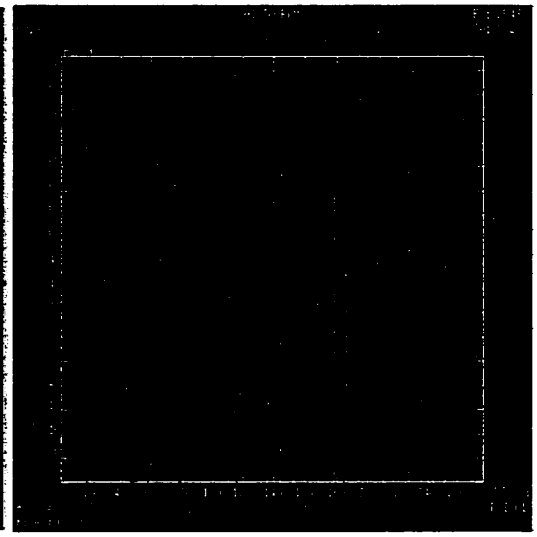

Figure 23 - Distribution of T2* slopes by pixel (Patient S02)

Table 7 - T2* distribution (narrow/wide) versus T2* slope (oxygenation), log DCE input function, serum hemoglobin, serum hematocrit

T2* Distribution	T2* slope (1/ms) (Mean±S.E.)	Input Function ($log\text{-}sec^{-1}$) (Mean±S.E.)	Serum Hgb mg/L (Mean±S.E.)	Serum Hct (Mean±S.E.)
Narrow	-0.023 ± 0.004	13.9 ± 9.3	156.3 ± 5.0	0.46 ± 0.02
Wide	-0.012 ± 0.005	50.6 ± 36.9	140.3 ± 7.3	0.41 ± 0.01

Table 8 - Narrow and wide T2* distribution by node status at diagnosis

Node / T2* distrib	Negative	Positive
NARROW	4	0
WIDE	2	4

Table 9 - Narrow and wide T2* distribution by tumor stage

Stage / Large Vessel %	1	2	3	4
LOW	1	3	0	0
HIGH	0	2	3	1

Sample T2* distribution on MR are shown in Figures 24a (wide distribution) and 24b (narrow distribution)

Figure 24a - Wide distribution of T2* values

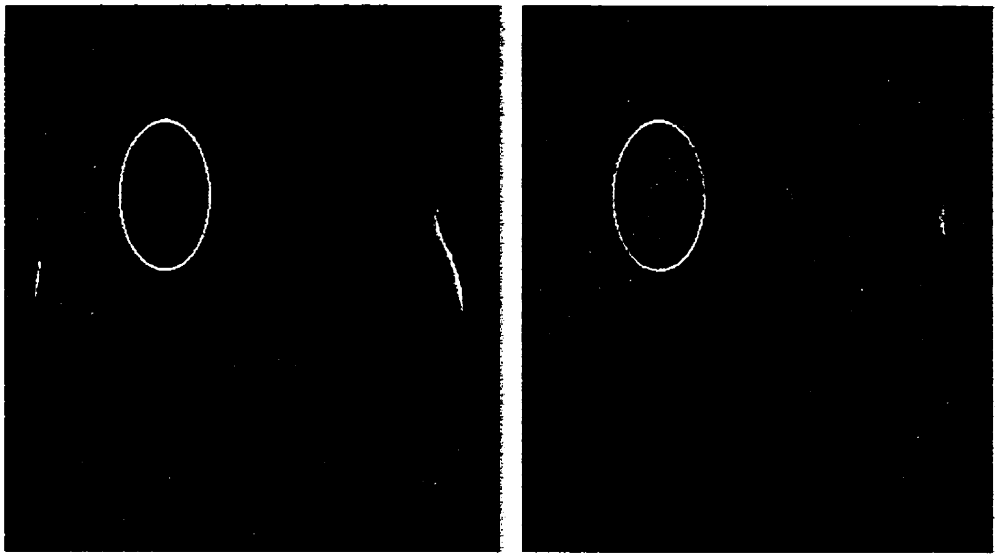

Figure 24b - Narrow distribution of T2* values

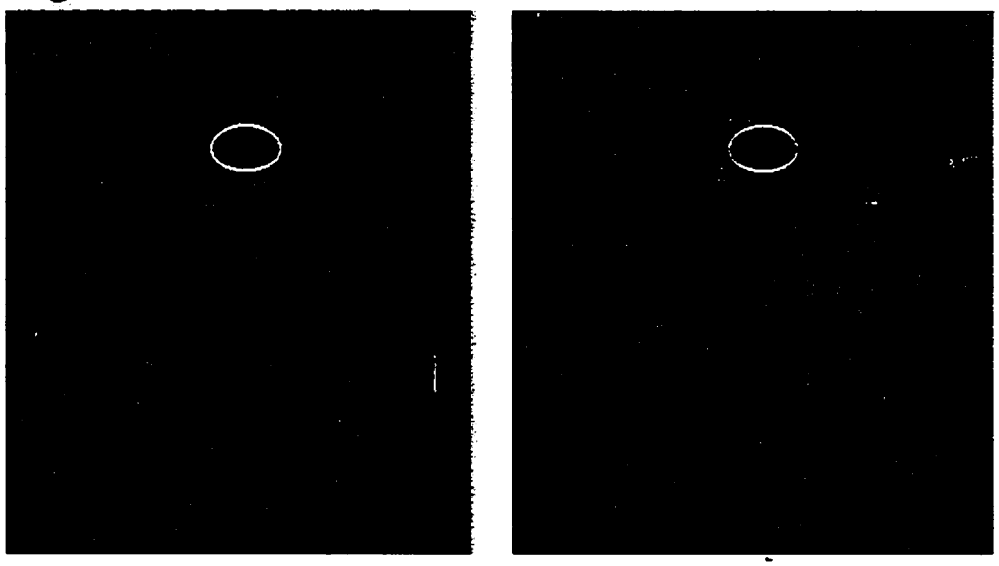

White line demarcates the approximate tumor boundary

Sentinel Node Study in Pigs

Interstitial injection of Combidex resulted in loss of signal in regional nodes at either dose level, however, more nodes were detected using the higher dose (Table 10.) The lower Combidex dose detected neck nodes in the jugulo-omohyoid and jugulo-digastric areas. The higher Combidex dose also detected more distal nodes in the spinal accessory and superficial cervical chains. In the interstitial injections of the stifle, both Combidex doses detected superficial and deep inguinal nodes.

Table 10 - Number of nodes visualized

Combidex Dose	Injection Location	Total Nodes Visualized
10 mg/ml (n=10)	Tongue	35
10 mg/ml (n=10)	Stifle	15
0.4 mg/ml (n=4)	Tongue	8
0.4 mg/ml (n=4)	Stifle	4

Individual nodes and their anatomical location were easily identified on MR images, regardless of dose (see examples, Figure 25).

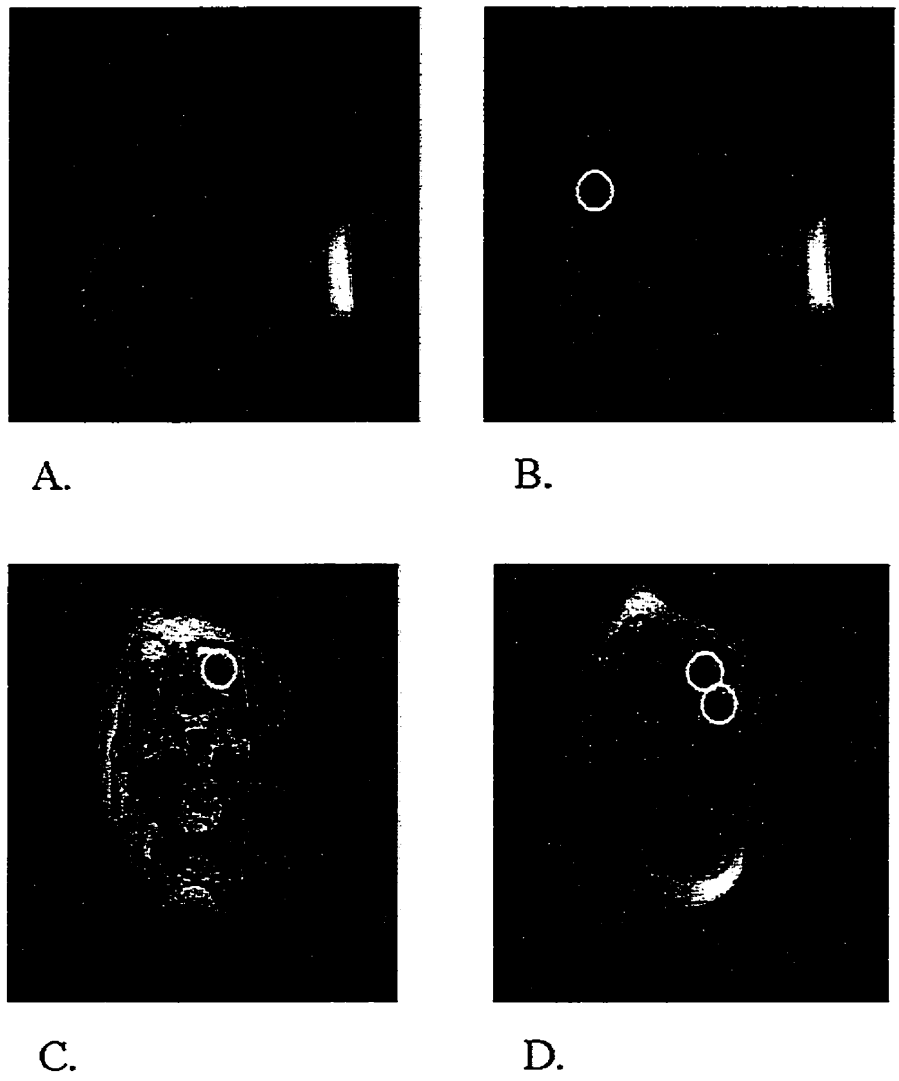

Figure 25 - MRI images of pig sentinel node identification. A) pre-contrast, sagittal image, B) post contrast, sagittal image, C) post contrast, axial image, D) post contrast, axial image. White circles indicate sentinel node(s).

Signal intensity decreased over time in all nodal locations, indicating continued incorporation of Combidex into the nodes. Nodal slice area correspondingly increased over time reflecting the susceptibility artifact resulting from local collection of Combidex (Figure 26.)

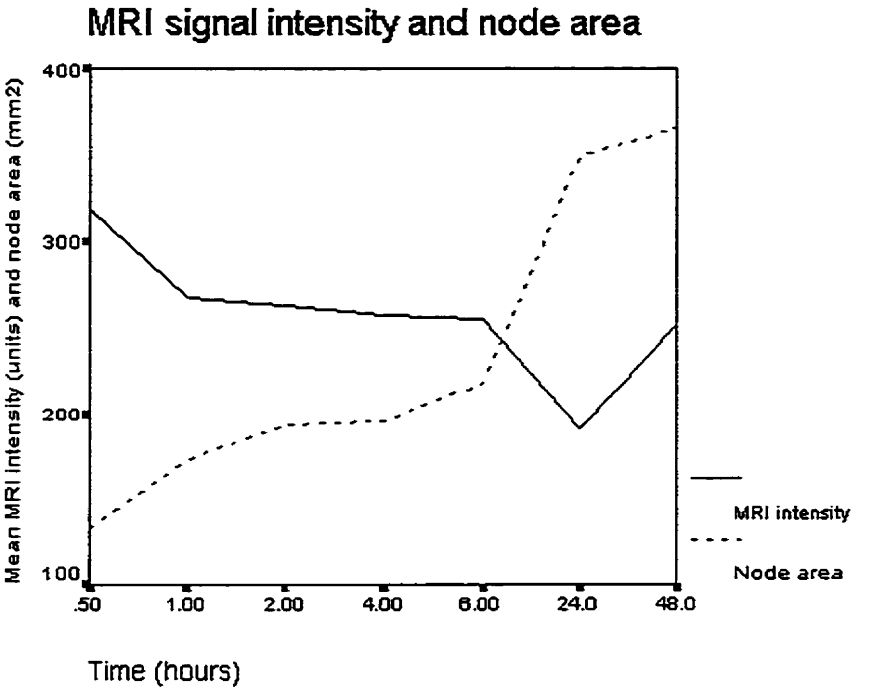

Figure 26 - MRI signal intensity and node image area by time.

Sentinel nodes were identified as the first node(s) to show susceptibility artifact (signal loss) on MR. At the high dose for the stifle injection, 1 sentinel node was identified in each of the 10 nodal drainage areas injected whereas in the tongue, 13 sentinel nodes were identified over the 10 neck drainage areas. All of these nodes were mapped as sentinel nodes using the isosulfan blue dye method. At the high dose in the tongue, two

additional sentinel nodes were identified by MRI that were not similarly identified by the isosulfan method. In the 4 stifle drainage area of pigs receiving the lower dose of Combidex, 4 nodes were detected in total, of which 3 were identified as sentinel nodes by both MRI and isosulfan blue. In the lymph drainage regions of the tongue in lower dose animals, 10 nodes were detected by MRI, 6 of which were identified as sentinel nodes by both methods. There were two additional nodes in the neck identified by MRI as sentinel nodes but not by the isosulfan method. A comparison of actual slice diameter of nodes (125-240 mm^2) compared to the MRI measured slice diameters demonstrated that MRI imaging with the high dose of Combidex overestimated nodal size (260±170 mm^2) while imaging with the lower dose produced a smaller node diameter (117±76 mm^2.) See Figures 27 and 28 for photographs of the dye SNB and Combidex SNB results *in vivo*. Complete sentinel node data can be found in Appendix H.

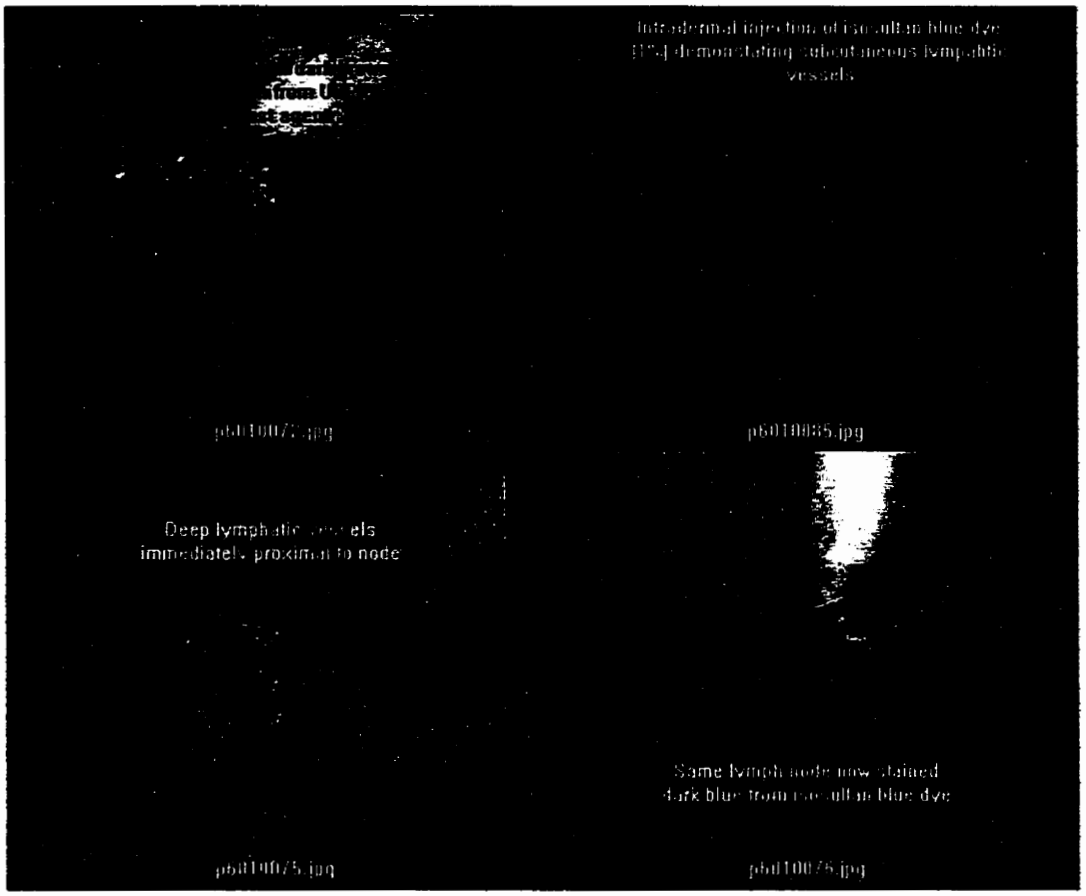

Figure 27 - In vivo photographs during sentinel node studies

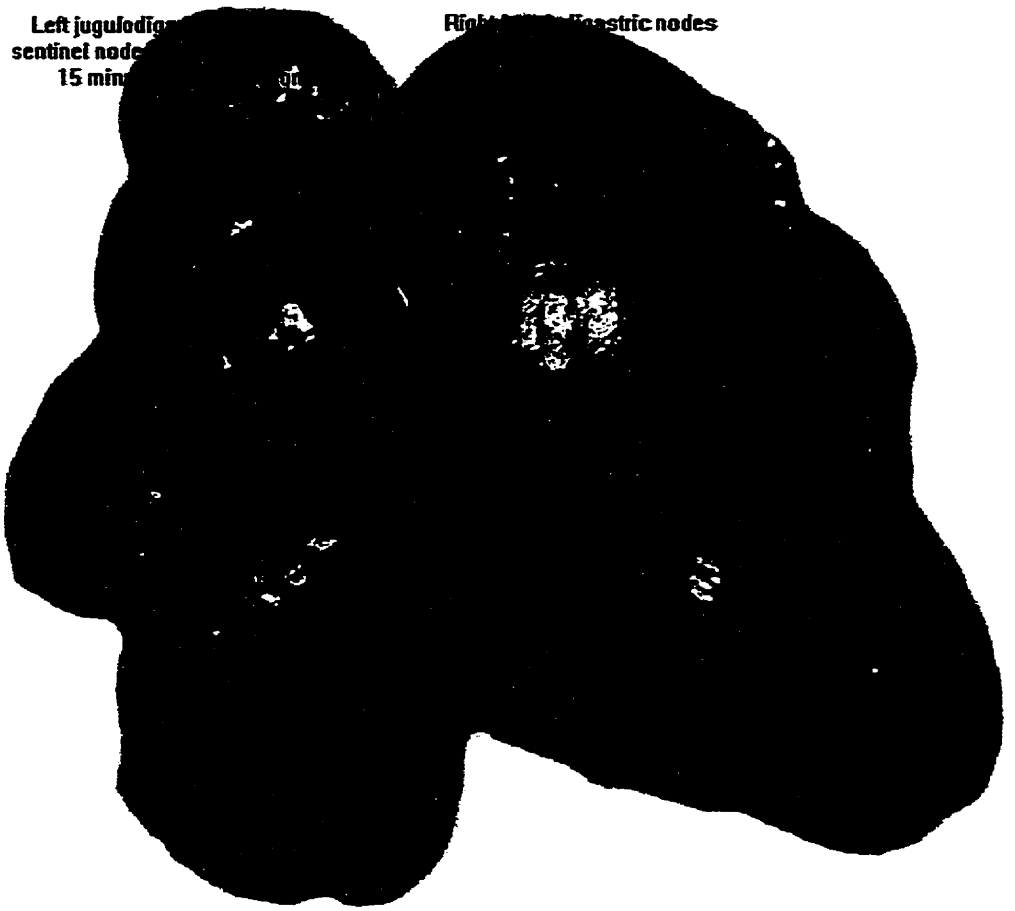

Figure 28- Photograph of experimental and control nodes *in vivo* (0.4 mg/ml contrast at t = 30 minutes.)

Discussion

The goal of the present study was to determine whether magnetic resonance imaging (MRI) has the ability to provide information that could have predictive utility in the determination of tumor treatment and patient prognosis. The three specific lines of investigation were: 1) dynamic contrast enhanced (DCE) MRI as a measure of tumor microvascularity, 2) blood oxygen level dependent (BOLD) MRI as a measure of tumor oxygenation, and 3) the novel use of an investigational ultrasmall particulate iron oxide (USPIO) contrast agent for the preoperative detection of sentinel nodes.

Rabbit VX-2 tumor models

Under the conditions in this experiment, the VX-2 tumors demonstrated very rapid growth in accordance with the report by Cochran, et al (140). Each of the tumors developed one or more area of central necrosis. Tumor necrosis can be a result of destruction of tumor cells by killer lymphocytes, through tumor necrosis factor excreted by triggered monocytes/macrophages, or from cell hypoxia. Hypoxia, in fast growing tumors, can be a result of the tumor outgrowing its blood supply through inadequate angiogenesis or excessive cell metabolism (141).

Rabbit DCE study

The DCE plots in the present study are consistent with those obtained from other clinical and experimental models (99, 142, 143). The DCE curve had three components, each of which represented a different kinetic function (97, 98). The initial rise component represents the time when the contrast agent is at its greatest concentration difference between intravascular and extravascular components, and its slope is representative of the rate of transfer between these two components, with contrast in the capillaries and extracellular space providing the increased MRI signal. The amplitude of the intensity change is indicative of the fraction of extracellular volume in the tissue. The final phase, known as the distribution or wash-out phase, results from loss of contrast through equilibration of the contrast to the vascular component as renal excretion proceeds and through lymphatic drainage. The variability in the shape of the curve reflects the varying amounts that each function plays in the overall DCE process.

In the present study, the rabbit VX-2 tumors the developed central necrosis likely a result of the loss vascular supply as demonstrated by a lack of contrast agent uptake in these areas. In the proliferating tumor edge, vascular supply remained good and the contrast agent was available for transfer into the extravascular space.

The slope of the uptake function in the rabbit VX-2 tumors was extremely high, partly as a function of the small overall vascular volume. Since the temporal resolution of the

sequences used was limited to 12 seconds or approximately 30-50% of the time required for complete uptake, the slope values may not be reliable. To increase the temporal resolution, a magnet of higher field strength with inherently increased signal to noise ratio would be required. The amplitude and the slope of the distribution function were more reliable measures in this animal model.

Normal muscle typically demonstrates little or no contrast enhancement so that the increased enhancement demonstrated in muscle tissue immediately surrounding the non-encapsulated tumor likely reflected the insidious infiltration of tumor cells into the adjacent area (see Figure 1.) The increase in the distribution slope (from a negative to positive value) of the tumor ROI over time indicated that the contrast agent was less able to leave the extracellular space resulting in pooling of the contrast. This could have been due to either greatly increased tumor cell population compared to available vessels for reuptake and/or decreased lymphatic uptake. The relative contributions for either process could not be extracted mathematically from the DCE curves in the rabbits. This would require reliable measures of input function as well monitoring intravascular contrast agent loss over time and obtaining this data would have required a higher field strength magnet.

Blood Oxygen Level Dependent MRI in Rabbit VX-2 Model

There have been no previously published reports of the use of BOLD MRI to measure relative tumor oxygenation. In the present VX-2 tumor model study, the relative

oxygenation levels in the proliferating tumor boundary were maintained over time. This was likely the result of tumor cells invading well oxygenated adjacent muscle and obtaining adequate oxygenation by diffusion largely from pre-existing vessels. The extremely rapid tumor expansion rate would have reduced the chances of developing of a well established tumor vascular supply. The internal areas of the tumor demonstrated reduced oxygenation very early reflecting an overtaxing of the available blood supply. The unique observation from the present study of simultaneous changes in the DCE distribution function (a reflection of vascular supply) and the decreases in oxygenation suggests that the tumor cell mass was outgrowing the local blood supply. This would result in hypoxia and ultimately cell death, as observed in the necrotic areas filled with sanguinous fluid and cell debris. VX-2 tumors show remarkable growth over a three week period which is a function of a short cell doubling time (approximately 1.5d) (140). The mathematical model of hypoxia and necrosis suggested by Måseide and Rofstad (141), based on the lifetime of hypoxic cells and their doubling time, fits well with observations in the VX-2 tumor model.

Microvascular Density in Archived HNSCC Tissue

CD-34 reacts with a transmembrane glycoprotein found on hematopoietic stem cell and endothelial cells and has been used to determine microvessel density. It is thought that CD-34 might play a role in intercellular adhesion (144). Although microvascular density has been studied by many investigators as a predictive marker for HNSCC patient

survival and for tumor recurrence(19, 43-46), microvascular density has not been shown to be related to the finding of nodal metastases (19, 145-148) or tumor histological progression (149-152). As indicated by Moriyama (19), the use of a single prognostic factor must be tempered with the fact that in all published studies there were patients with low microvessel counts and/or low angiogenic markers that had poor survival, positive nodes, and highly dysplastic nodes.

Neither the Weidner nor the International Consensus methods for calculating microvessel density (27;47) have made any attempt to normalize the microvascular density to compensate for tumor heterogeneity nor has there been any attempt to consider vessel size. As in the present study, most of the HNSCC studies of microvascular density have relied mainly on archived tissue specimens obtained at the time of surgical resection. It has not been demonstrated that tissue obtained at biopsy in these patients would have provided equivalent measures of microvessel density in comparison to surgical specimens, especially given the heterogeneity of many tumors and their blood supply. Without this validation, the use of microvessel density measurement must be restricted to providing information only after the primary treatment regimen has been set and it could not be used as a predictor of prognosis in patients undergoing primary radiation or chemotherapy treatment (149.)

There are no studies indicating the use of vessel size measurements to better define the microvessel density parameter. The microvasculature is important to continued tumor

growth since tumors with a diameter greater than approximately 3 mm cannot rely on simple peripheral diffusion of nutrients and oxygen. In the present study, there were an increasing number of larger microvessels (>25 μm) per high power field (HPF) as tumor diameter increased and these larger vessels also represented an increasing percentage of the total population of vessels. Larger tumors require enhanced nutrient supply. The increasing vessel size may simply indicate increased vascular organization within the tumor over time, with arterioles acting as a feeding network to the smaller capillaries. Smaller tumors may be able to rely on the lower flow capillary network alone.

A possible explanation for the relationship between the absolute number of, and percent distribution of large vessels in the tumors and the development of lymphatic metastasis shown in the present study is less clear. Despite the significant role of the lymphatic system in the propagation of metastasis in HNSCC and breast tumors, over the past ten years, there have been over 3000 publications relating to angiogenesis and tumors while there have only been 9 relating to lymphangiogenesis and tumors. What authors refer to as angiogenesis is perhaps more correctly called hemangiogenesis. Witte and coworkers have written an excellent review on the concept of lymphangiogenesis (153). Lymphangiogenesis is an active process as demonstrated in an experiment by Paavonen et al (154), where new lymphatic vessels were demonstrated to sprout from existing lymphatic vessels in wound edges. In the normal situation however, lymphatic endothelium, like vascular endothelium, is, from a normal proliferative turnover point of view, relatively inactive (153). Witte's criticism of the microvascular density work is that

little has been done to correlate blood flow with blood vessel density and tumor characteristics. In tumors such as Kaposi's sarcoma, blood flow stasis has been demonstrated (153). Combined with the fact that up to very recently it has not been possible to positively identify and separate blood from lymphatic vessels how then can it be implied that hemoangiogenesis specifically is the prognostically valid variable? Structurally, the lymphatic vessel's lack of a basement membrane and their porous nature would provide a prime location for invasion by the metastatic fraction of tumor cells. Perhaps a better predictor of nodal metastasis in HNSCC would be lymphatic vessel microdensity. Witte indicated that advances in MRI might be able to elucidate blood and lymphatic flow in tumors (153). While members of the vascular endothelial growth factor (VEGF) family are released during periods of hypoxia, only VEGF-3 receptors are restricted to lymphatic endothelium. VEGF-3 expression is not increased during hypoxia (155) but is significantly enhanced in vascular tumors (156, 157). It is unclear whether the lymphatic vessels seen on microscopic section of tumors are newly formed or pre-exiting vessels that were simply incorporated into the tumor as it grows. Paavoenen and coworkers (154) very recently demonstrated new lymphatic vessels sprouting from pre-existing lymphatic vessels in tissue edges in incisional skin wounds in pigs and in chronic granulomatous tissue in humans. In both cases, the vessels stained for VEGF-3 receptors. Increased hemoangiogenesis in a tumor implies the necessity for additional lymphatics to drain fluid, protein, and lymphoid cells that exit the blood capillary network into the tumor's interstitial space. Increased interstitial pressure may well be a trigger for lymphangiogenesis. This has not been investigated. De Waal and coworkers (158)

determined that in both horizontal and vascular growth phase melanomas, there was no difference in the number of lymphatic vessels in comparison to normal adjacent tissue. They did not specifically stain for lymphatic vessels but used a double stain to identify blood vessels. In the deepest tumors, it appeared that the lymphatic vessels were compressed by the growing tumor.

In the present study, it is possible that lymphatic vessels represented a higher proportion of the stained larger vessels than of the smaller capillaries. Whether these are pre-existing or newly formed vessels is unclear from the microvascular density and vessel diameter measurements. Since both the size of tumor and the nodal status related to the percent of large vessels in a given tumor area, it is not surprising that tumor stage is similarly related since the latter is comprised of factors taken from tumor size, nodal status, and occurrence of distant metastases. None of the patients had distant metastasis at the time of diagnosis or treatment.

The finding that the increased small vessel size distribution was an independent predictor of increased patient survival and decreased probability of tumor recurrence has not been previously documented. A recent study using color Doppler measurements of cervical node metastasis in advanced HNSCC demonstrated that increased color pixel density (a measure of blood flow) was a predictor of reduced survival in patients treated with radiotherapy (87). Color Doppler is unable to measure capillary flow, so the pixel density related to larger vessel size (87). This is in agreement with the data from the present

study. A second report using CT contrast injection to measure tumor capillary perfusion failed to demonstrate a correlation with survival (110), which would corroborate Witte's (153) concern over the distinction between increased vessel number versus vessel perfusion. In the current study, the increased survival of patients with increased small vessel distribution might have also be related to differing tumor cell physiology between patients, with some tumor cells types triggering widespread capillary production and others promoting enlargement of pre-existing blood vessels, as a response to hypoxia (159). Such a factor might simultaneously influence tumor cell aggressiveness or metastasis. The neovascularization of the tumor by capillary growth may also be indicative of relatively consistent changes in oxygenation during tumor growth whereas areas containing a higher percentage of large vessels may have been exposed to acute periods of increased hypoxia requiring not just increased capillary coverage but also higher blood flow rates that could only be achieved with larger vessels. To date, no studies have studied how the process of angiogenesis affects changes in vessel size which would be useful as a correlate to of oxygenation and blood flow.

Dynamic Contrast Enhanced (DCE) MR in Patients

Increased contrast uptake by a tumor in comparison to normal tissue viewed by either CT or MRI has been known for many years, and is the basis for the expression 'contrast enhancing lesion' that is commonly reported by radiologist. While a gross measure of enhancement is useful for defining tumor boundaries and, in some cases, fingerprinting of

a specific tumor type, the calculation of the functions of DCE enhancement has provided additional physiologic information about tumors as demonstrated by many other groups (99, 100) although never in HNSCC. Unlike the rabbit VX-2 tumor model, the SCC tumors in patients demonstrated more consistent DCE functions in the ROI's from tumor center and periphery. No frank necrosis was seen in any of the patient tumors. There was sufficient temporal resolution to reliably measure the input or transfer function (intra- to extravascular) of the DCE curves. The span or total increase in contrast intensity theoretically relates to the distribution volume or physiologic space for diffusion and in this group of patients it was statically correlated with tumor size. The distribution function (the last phase of the DCE curve) relates to the loss of contrast through renal elimination coupled with extracellular to intravascular concentration gradient and lymphatic drainage. In the present study the elimination function was significantly increased in patients with a greater number of large blood vessels in the tumor. The limiting factor in loss of contrast by renal excretion is likely not tumor vascular flow (since all patients had very high input functions) but rather renal elimination of the contrast agent. It would be expected that renal elimination would be relatively consistent (or randomly distributed) among these patients although specific renal function tests were not performed. If this assumption is valid then it would follow that the increase in the distribution function seen in these patients was related to increased lymphatic drainage. It would also imply that the larger vessels seen in larger tumors were related to increased lymphatic drainage or were lymphatic vessels. Given that the present study has also demonstrated that increased number of large vessels are related to positive node status, it

is plausible that the availability of more lymphatic vessels provided increased locations for metastatic cell populations to infiltrate.

DCE by Pixel Analysis

Spatial resolution of MR images is a function of the field of view (FOV) and the matrix size, or the number of pixels in the two axis of the image. Since signal strength decreases with the FOV, the preference for increasing spatial resolution is limited in practice by increasing noise. Partial volume averaging is an effect seen in MRI that relates to spatial resolution. Partial volume effects result when more that one type of tissue is contained within any given location or pixel in the image. The value for the signal intensity in that pixel represents the intensities from the differing tissues. In typical DCE MR imaging, regions of interest (ROI's) on the image are selected based on anatomical criteria such as the tumor geometric centre. However, from a physiological viewpoint, defining boundaries in this manner may be less appropriate. For example, a tumor may develop a larger blood vessel in a particular area, but when the ROI of the region is chosen, the DCE parameters from the vessel are averaged into those of the surrounding area. This can result in 'softening' of the mathematical functions. Hawighorst et al (109) and others (107) have mapped the pixel values for each of the DCE components onto anatomical maps. Mathematically, DCE factors can be interdependent and it would be advantageous to describe the complete DCE functional curve at any pixel. Mathematical extraction of individual DCE curves from these average functions has recently been suggested to be

theoretically possible (160), but no clinical application has been attempted. In this present study clustering of like pixels based on the complete DCE function was accomplished using EvIdent software that performs hierarchical function clustering on temporally resolved MR images. The software was originally designed for use with functional MRI (fMRI) mapping. Quantitative comparison and statistical analysis was not performed due to the wide variation of cluster mapping between patients. However, clustering analyses demonstrated that there were differences in DCE function curves between individual tumor pixels in any given tumor and that the pixels demonstrated clustering, indicating that there are large subsets of physiologically similar areas (based on DCE functionality) within the whole tumor. These subset areas may represent important markers of tumor behaviour (such as increased blood or lymphatic flow), but further study with increased patient numbers and more defined mathematically modeling will be required.

If predictive physiological parameters of tumors can be reliable measured using MRI, the technique would have many clinical advantages: 1) essentially non-invasive (except for the injection of contrast), 2) could be performed in the pre-treatment period, 3) could be repeated as tumor treatment progresses in radiotherapy and chemotherapy, and 4) provides a complete three dimensional physiologically based map of the tumor.

Blood Oxygen Level Dependent (BOLD) MR by ROI Average

Tumor oxygenation has been reported to be an important factor in predicting the natural

behaviour of tumors and in defining their therapy (111-113,161). Tumor oxygenation is related to the adequacy of the blood supply and to tumor oxygen requirements (141). One of the main triggers for angiogenesis is hypoxia (159), so that as tumors grow and cell clusters become less well oxygenated as they move away from any preexisting blood vessel (162), a signal to form new vessels is produced (25, 26). In the present study, BOLD MR imaging of relative oxygenation levels demonstrated a wide range of tumor oxygenation between patients as would be expected since each tumor has its own metabolic requirements and blood (oxygen) supply. Oxygenation as a function of tumor size has not be previously measured but was demonstrated in this study. The greater number of large vessels seen in larger tumors combined with increased oxygenation would indicate that these larger vessels may provide increased oxygen supply to the tumor cells through increased perfusion. Although capillaries (diameters of <10μm) are often thought to be the main source for oxygen diffusion to cells, Swain and Pittman (163) demonstrated that over 60% of oxygen diffusion occurs in the arterioles (20-60μm) with the remainder occurring in capillaries. This corresponds well to the present study that showed increased oxygenation in larger tumors with high numbers of larger vessels (arterioles) concurrent with a relatively constant number of smaller vessels or capillaries.

Another factor that must be considered in the discussion of oxygenation in tumors is the ability of the patient's blood to carry oxygen. Hematocrit or packed cell volume (PCV) is a measure of the concentration of red blood cells in the blood, while hemoglobin (Hgb)

concentration is an indication of each erythrocyte's ability to carry oxygen. Depending on the specific cause, anemia, or the decrease of oxygen-carrying capacity by the blood, may present with various combinations of PVC and Hgb values. In patients with malignancy, anemia is often related to occult bleeding or poor nutritional status from anorexia. In patients with HNSCC decreased food intake may be related to pain or mechanical difficulties with chewing or swallowing. Cachexia, or wasting syndrome, is a relatively common occurrence in malignancy. Reduced hemoglobin has been demonstrated (164-166). Severely anemic patients (Hgb <11 g/dL) with HNSCC and those who continue to smoke have shown decreased tumor oxygenation using the polarography method (167). In the present study, advanced tumor stage was related to decreased PCV and Hgb. Despite the fact that patients with the largest tumors had the lowest blood oxygen carrying capacities, their tumors showed the highest relative oxygenation levels. This was likely due to increased tumor blood flow through the larger vessels found in the larger tumors.

BOLD MR Imaging by Pixel Analysis

Measurements of oxygen tension in tumors and their metastases have been reported and up until recently, polarographic electrode techniques were employed (114,161,168,169). In this technique, a small diameter (18 gauge), precalibrated electrode is introduced into the tissue and a series of oxygen tension measurements are made as the electrode is slowly moved along a tract. Multiple tracts are measured and the data is combined into histograms of oxygen tension values. Studies in patients with HNSCC have demonstrated

a correlation between increased tumor hypoxia and poorer outcome (114,161,168,169). Dietz and coworkers (170) have also shown that tumor oxygenation changes during the first week of radiation therapy and Lyng and associates have confirmed this (170,171) .

Determining oxygen tension with the polarographic technique limits the measurement to essentially one dimension, since only a limited number of tracts can be examined. This results in wide variances in oxygenation measurements and increases the uncertainty of using an individual patient's data as a direct predictor of that patient's prognosis (170). Given the heterogeneity of tumors, it would appear advantageous to be able to obtain at least a two dimensional picture (and ideally a three dimensional picture) of oxygen tension to make this measurement a more reliable predictor of tumor properties. Although histological markers of tumor oxygenation have been developed, the techniques are obviously invasive and would be subject to tumor heterogeneity and therefore biopsy bias. If surgical specimens are used to reduce this bias and increase three dimensional measurements, knowledge about the tumor cannot be obtained until after primary surgical treatment is initiated. Obviously this would prevent use of the technique for monitoring progression of radiotherapy or chemotherapy treatment. Magnetic resonance spectroscopy has recently been shown to correlate lactate levels (in human tumors) and water resonance (in rats) with tumor and metastasis oxygenation measured by polarographic methods(172-174). This present investigation is the first report of the use of BOLD imaging to study tumor oxygenation in humans. MR methods have a number of advantages including being non-invasive and allowing measurements in three

dimensions. Pixel analysis of the relative oxygenation of the tumors in the current study demonstrated that tumors have varying degrees of relative oxygenation distribution, and that wide distributions related to the finding of positive nodes and to tumor stage. These data support the previous observations of oxygenation heterogeneity made by polarography (114,161,168,169). Wide distribution of relative oxygenation levels also correlated with the DCE parameter that reflects increased blood flow (increased input function), and, moreover, related to this increased flow is that these tumors also have the highest overall relative oxygen saturation levels. Wider distribution of oxygenation values implies that there are areas within the tumor with varying metabolic requirements or with varying blood supplies or both. Tumor cell metabolism was not measured, but the wider distributions were associated with higher percentage of larger vessels. This would follow from the previously noted observation that arterioles are the site for significant oxygen diffusion, and their localization may be represented by the hot-spots of oxygenation noted on the T2* pixel maps.

Tumor oxygenation is an important factor in the treatment of tumors by chemotherapy and radiation therapy. Chemotherapeutic agents have been classified by their relative cytotoxicities to cells that are hypoxic or well oxygenated (175). It may be important to use tumor oxygen saturation measurement as a means to optimize the selection of chemotherapy agents. It has been know for many years that tumor cell killing by radiotherapy is a function of tumor oxygenation (162). It is now understood that this cytotoxicity is based on the production of toxic atomic species including free oxygen

radicals that in turn affect a variety of cell pathways or nucleic acid structure. Recent studies have confirmed that head and neck tumors that have a lower hypoxic fraction may respond better to radiotherapy and have better overall outcome(112,114,161,168). In a preliminary study by Giatromanolaki and coworkers (176), the success of treatment of HNSCC by chemotherapy was also related to tumor vascularization. A study in patients with cervical cancer demonstrated that tumor hypoxia can also be a predictor of metastases (113). More recent work has been aimed at increased tumor oxygenation during radiotherapy either pharmacologically (using nicotinamide) or by having the patient breathe carbogen (95% O_2/5% CO_2) (93,177-179). Initial results look promising with an increase in loco-regional control. BOLD MRI would be an ideal means of investigating tumor oxygenation both before and during treatment by chemotherapy or radiation therapy, and since BOLD relies on inherent tissue contrast, studies could be repeated frequently as treatment progresses.

The major drawback to BOLD MR imaging is that at present it provides only a relative measure of oxygen saturation in the tumor as represented by the conversion of hemoglobin to deoxyhemoglobin. Over the past year, a number of biocompatible fibre optic microprobe oxygenation measurement systems have appeared on the marketplace (Compte GmbH, Hanover, and OceanOptics, Duiven, The Netherlands.) These systems are compatible with MR instrumentation since there are no electrical or metallic components required at the measuring tip and could be used to calibrate the BOLD MR relative measurements to absolute oxygenation values.

Sentinel Node in Pigs

The present study has demonstrated that Combidex (ultrasmall particles of iron oxide, USPIO) may be a valuable agent for the detection of sentinel nodes, especially in the head and neck. Combidex (also known as AMI-227) is a low toxicity, 20 nm diameter, dextran coated iron oxide prepared for reconstitution as a colloid (180,181). Previous work with other iron oxide contrast agents have been focused on their intravenous or interstitial use as agents to determine whether nodes were metastatic (130-132,182,183). Studies by Anzai and Prince (184-186) demonstrated that macrophages in human nodes take up USPIO and that this contrast may allow for differentiation of normal and metastatic nodes. A paper by Hoffman et al demonstrated the use of intravenous Combidex in patients with HNSCC (187). They showed that malignant nodes in the neck could be identified based on their contrast filling characteristics, however, nodes that could not be identified because of their small size by standard MRI could also not be identified using IV Combidex. This was almost certainly due to the relatively small concentration of Combidex that collects in nodes following intravenous injection. USPIO agents, by either mode of injection could detect grossly metastatic nodes based on their filling criteria (187). However, continued study of these agents, exclusively by intravenous injection, has not been very successful in the imaging of neck nodes (89). All of the experimental studies used the contrast agent for non-specific lymphangiography with no concern about temporal changes or specific node ordering. In a study by Jamie Rogers et al (133) from Advanced Magnetics, the term sentinel node was used arbitrarily to identify any single

node detected using a very low dose of Combidex in three rats (133). However, even at the low dose the authors implied that multiple nodes demonstrated contrast uptake. Since the study was limited to a single MR image at 24 hours, no information could be obtained about node filling order which is critical to the establishment of true sentinel node status as noted by two of the originators of the sentinel node technique, Morton and Ollila (75), in their detailed evaluation of sentinel node methodology. Furthermore, it can not be assumed that the closest of any number of nodes detected is the sentinel node(188). It has been demonstrated that detection using the radio-colloid agents is highly dependent on the type of agent and the time interval between injection and detection (75,76). The longer the time period and the higher the dose the greater number of nodes that are radioactive and can be detected. As Morton and Ollila (75) importantly point out, not every node that is radioactive is a sentinel node and they continue to use isosulfan blue dye as the gold standard. For all these reasons, isosulfan dye was used as the gold standard in the present project. Applying the same radiocolloid reasoning to MRI lymphangiography, not every node that shows contrast change following interstitial injection of contrast, is a sentinel node, as suggested by Rogers et al(133). Rather the sentinel node is the *first* node or nodes draining the site, so that temporally resolved imaging is critical to the MR sentinel node methodology, until at least such a time that extensive clinical application defines a precise protocol.

The potential for the evolution of MR sentinel node methodology from concept to a clinical tool inspired the current study to reexamine the use of USPIO as a contrast agent specifically for the MRI detection of sentinel nodes. Although the discussion here is centred around patients with HNSCC, this MRI sentinel node technique would also be valid for use in patients with breast cancer or melanomas. While the present study can not claim to be the first to suggest MR sentinel lymphography, it certainly is the first to prove its theory, demonstrate its pre-clinical utility, and compare its reliability to currently accepted 'gold standard' method.

In the present study, there were two nodes in each group that were demonstrated to be sentinel nodes by the MRI technique but not by the gold standard isosulfan blue. Theoretically these nodes would be considered as false positives. Sentinel node techniques have been noted to require a fairly lengthy learning curve to achieve good clinical reproducibility and are highly dependent on dose of agents and timing. The most likely reason for the discrepancy between the two methods used in the present study was simply lack of operator experience in the SNB technique. On the other hand, it is also possible that the temporal resolution in the MR method was insufficient to detect the absolute first node showing contrast change although this is less likely. There remains the possibility that the MRI results are in fact correct, that in fact there were two false negative results in the isosulfan blue dye method. Similar discrepancies between isosulfan dye and radiocolloid methods have also been reported (72,73). This anomaly will only be solved with additional testing and fine tuning of the MRI methodology preferably in an

early clinical trial.

Sentinel node techniques for HNSCC have been reported but its use has proven to be more difficult to implement than in breast cancer or melanoma for a number of technical reasons. These include unwanted tissue staining through diffusion of the dye from the site of injection and the lymphatics (189) and radiation from the injection site overwhelming the smaller signal from any closely associated sentinel nodes (69-71). There is continued debate over what the minimum gamma count of a node should be to constitute it as a sentinel node (75,79). The MRI technique described in this study improves considerably on the other methods. The volume of interstitial USPIO required for the detection of nodes is very small in comparison to the isosulfan blue dye method and does not cause local or distant staining of tissues that would interfere with dissection at the tumor site or in the neck. The local artifact from the contrast agent at the injection site is reduced and combined with MR imaging that uses thin slices and good spatial resolution, any close nodes could be easily distinguished from the injection site. If there was clinical concern about nodes juxtaposed with the injection site, after waiting twenty four hours, the agent is almost completely removed from the injection site, and any nodes could be imaged.

These methodological improvements are perhaps less important than the fact that MRI sentinel node detection is minimally invasive, can be accomplished preoperatively, provides positive node identification at the time of surgery by color deposition of the USPIO, and allows imaging with outstanding spatial resolution and soft tissue contrast

for detailed anatomical mapping. These characteristics present interesting possibilities. With precise anatomical information about sentinel node and the confirmatory coloration from Combidex deposition, it may be possible to perform a simple excision of the sentinel node(s) for histological study. With the current interest in minimally invasive techniques, MR sentinel node identification could also be followed by interventional MR guided FNA or biopsy of the sentinel node in a similar fashion to that demonstrated using CT guidance(190) in HNSCC. Laparoscopic excision of axillary nodes have been demonstrated(191). Pretreatment histological diagnosis of sentinel node status would have obvious implications in the selection of treatment plans for patients with HNSCC. Preoperative MR sentinel node identification would provide information to the surgeon for adjusting the neck node dissection level. If the sentinel node(s) contained only micrometastasis, it might be demonstrated that only that node(s) needs to be removed for adequate treatment of the neck. It is interesting that in 60% of breast cancer patients, the sentinel node is the only positive node(56) and therefore it may be possible to identify patients that do not require wide lymph node dissection. Superselective lymph node dissection could also be done at lymph node levels specifically identified to incorporate the sentinel node(s). MR sentinel node identification would also provide similarly important information for planning of radiation treatment fields.

Conclusions

Based on the results of the present study the following original hypotheses can be accepted:

1) that the rabbit VX-2 squamous cell carcinoma model demonstrated basic properties of dynamic contrast enhanced and BOLD MR, 3) that in patients with HNSCC, the distribution of vessel size in a tumor was an independent measure of patient outcome, tumor stage, and nodal metastasis, 4) that DCE and BOLD MRI was technically feasible in HNSCC, 7) that since HNSCC tumors displayed histological heterogeneity they will demonstrate heterogeneity in both DCE and BOLD analysis, 6) that BOLD measurements of relative tumor oxygenation was correlated to tumor vascular supply and, 8) that USPIO contrast agent behaved similarly to radiocolloid materials and was able to demonstrate sentinel node identification. The hypothesis 2) that in patients with HNSCC, tumor microvascular density would be a measure of patient outcome, tumor stage, and nodal metastasis, must be rejected. Hypothesis 5) that DCE functions would correlate with tumor microvascular density and distribution of vessel size must be rejected since not all DCE functions showed correlation, however specific DCE functions namely, amplitude and distribution did correlate with number of large vessels in the tumor.

Rabbit VX-2 tumors appeared to be a valid model for the further investigation of both DCE and BOLD MRI, and should be further improved by enhancing temporal resolution of DCE sequences. Variables associated with microvessel size distribution were related to

tumor characteristics as well as patient survival and recurrence and these variables could, in part, be described by the amplitude and distribution functions of DCE MRI. The sole DCE function that related, in part, to lymphatic flow was correlated with nodal status. BOLD analysis confirmed that tumors can be heterogenous in relative oxygenation values and that these oxygenation gradients are related to DCE input function and nodal status. Finally, identification of sentinel nodes by MRI lymphangiography using the USPIO contrast agent, Combidex, is technically feasible and shows good correlation with the isosulfan blue dye method.

In summary, this current study has demonstrated that minimally invasive techniques based on magnetic resonance imaging have a supportive role to play in the evaluation and possibly the management of head and neck squamous cell carcinoma.

Reference List

(1) Hoffman HT, Karnell LH, Funk GF, Robinson RA, Menck HR. National cancer data base report on cancer of the head and neck. Arch Otolaryngol Head Neck 1999; 124:951-962.

(2) National Cancer Institute of Canada. Canadian Cancer Statistics 2000. 2000.

(3) La Vecchia C, Tavani A, Franceschi S, Levi F, Corrao G, Negri E. Epidemiology and prevention of oral cancer. Oral Oncology 33[5], 302-312. 1997.

(4) Brunin F, Mosseri V, Jaulerry C, Point D, Cosset J, Rodriguez J. Cancer of the base of the tongue: past and future. Head & Neck 1999; 21:751-759.

(5) Cancer Statistics. CA Cancer Journal for Clinicians 1999; 49(1):8-31.

(6) Correa A, Burkey B. Current options in management of head and neck cancer patients. Medical Clinics of North America 1999; 83(1):235-246.

(7) Yousem DM, Montone KT. Head and neck lesions. Radiologic-pathologic correlations. Radiol Clin North Am 1998; 36(5):983-1014, vii.

(8) Denoix P, Schwartz D. Règlés générales de classification des cancer et de présenation des résultats thérapeutique. Academia Chirurgerie 1959; 85:415-424.

(9) O'Brien CJ, Traynor S, McNeil E, McMahon J, Chaplin J. The use of clinical criteria alone in the management of the clinically negative neck among patients with squamous cell carcinoma of the oral cavity and oropharynx. Archives of Otolaryngology and Head and Neck Surgery 2000; 126:360-365.

(10) Yueh B, Feinstein AR, Weaver EM, Sasaki CT, Concato J. Prognostic staging system for recurrent, persistent, and second primary cancers of the oral cavity. Arch Otolaryngol Head Neck 1998; 124:975-981.

(11) Yii N, Patel S, Rhys-Evans P, Breach N. Management of the N_0neck in early cancer of the oral tongue. Clinical in Otolaryngology 1998; 24:75-79.

(12) Firth NA, Reade PC. The prognosis of oral mucosal squamous cell carcinomas : A comparison of clinical and histopathological grading and of laminin and type IV collagen staining. Australian Dental Journal 1999; 41(2):83-86.

(13) Byers R, Wolf P, Ballantyne A. Rationale for elective modified neck dissection. Head and Neck Surgery 1988; 10:160-167.

(14) Strahan D. Head and neck cancers. 1999.

(15) Adelstein D. Recent randomized trails of chemoradiation in the management of locally advanced head and neck cancer. Current Opinion in Oncology 1998; 10:213-218.

(16) Resser J, Carbone D. Immunotherapy of head and neck cancer. Current Opinion in Oncology 1998; 10:226-232.

(17) Mukherji SK, Neelon B, Gapany M, McCartney W. Evaluation of ^{201}Tl SPECT for predicting early treatment response in patients with squamous cells carcinoma of the extracranial head and neck treated with nonsurgical organ preservation therapy: initial results. Journal of Computer Assisted Tomography 2000; 24(1):146-151.

(18) Liu M, Weynand R, Delos M, Marbaix E. Prognostic factors in squamous cell carcinomas of the head and neck. Acta Otology Rhinology Laryngology of Belgium 1999; 53:155-160.

(19) Moriyama M, Kumagai S, Kawashiri S, Kojima K, Kakihara K, Yamamoto E. Immunohistochemical study of tumor angiogenesis in oral squamous cell carcinoma. Oral Oncology 1997; 33(5):369-374.

(20) Folkman J. Tumor angiogenesis: therapeutic implications. New England Journal of Medicine 1971; 285:1182-1186.

(21) Folkman J. Angiogenesis in cancer, vascular, rheumatoid, and other diseases. Nature Medicine 1995; 1(1):27-31.

(22) Petruzzelli GJ. Tumor angiogenesis. Head & Neck 1996; 18:283-291.

(23) Gasparini G. Angiogenesis research up to 1996. A commentary on the state of art and suggestions for future studies. European Journal of Cancer 1996; 32A(14):2379-2385.

(24) Fox S. Tumor angiogenesis and prognosis. Histopathology 1997; 30:294-301.

(25) Ferrara N, Houck K, Jakeman LB, Leung DW. Molecular and biological properties of the vascular endothelial growth factor family of proteins. Endocrine Reviews 1992; 13(1):18-32.

(26) Ferrara N, Davis-Smyth T. The biology of vascular endothelial growth factor. Endocrine Reviews 1997; 18(1):4-25.

(27) Weidner N, Semple J, Welch W, Folkman J. Tumor angiogenesis and metastasis - correlation in invasive breast carcinoma. New England Journal of Medicine 1991; 324(1):1-8.

(28) Goede V, Fleckenstein G, Dietrich M, Osmers RG, Kuhn W, Augustin HG. Prognostic value of angiogenesis in mammary tumors. Anticancer Research 1998; 18:2199-2202.

(29) de Jong JS, van Diest PJ, van der Valk P, Baak JP. Expression of growth factors, growth inhibiting factors, and their receptors in invasive breast cancer. I: An inventory in search of autocrine and paracrine loops. Journal of Pathology 1998; 184:44-52.

(30) Toi M, Kondo S, Suzuki H, Yamamoto Y, Inada K, Imazawa T et al. Quantitative analysis of vascular endothelial growth factor in primary breast cancer. Cancer 1996; 77(6):1101-1106.

(31) Macchiarini P, Fontanini G, Hardin MJ, Squartini F, Angeletti CA. Relation of neovascularization to metastasis of non-small-cell lung cancer. Lancet 1992; 340:145-146.

(32) Bremer G, Tiebosch A, van der Putten H, Schouten H, de Haan J, Arends J. Tumor angiogenesis : an independent prognostic parameter in cervical cancer. Am J Obstet Gynecol 1996; 1(1):126-131.

(33) Tjalma W, Van Marck E, Weyler J, Dirix L, Van Daele A, Goovaerts G et al. Quantification and prognostic relevance of angiogenic parameters in invasive cervical cancer. Br J Cancer 1997; 78(2):170-174.

(34) Salven P, Lymboussaki A, Heikkilä P, Jääskela-Saari H, Enholm B, Aase K et al. Vascular endothelial growth factors VEGF-B and VEGF-C are expressed in human tumors. American Journal of Pathology 1999; 153(1):103-108.

(35) Landriscina M, Cassano A, Ratto C, Longo R, Palazzotti B, Crucitti F et al. Quantitative analysis of basic fibroblast growth factor and vascular endothelial growth factor in human colorectal cancer. British Journal of Cancer 1998; 78(6):765-770.

(36) Danielson T, Rofstad EK. VEGF, bFGF, and EGF in the angiogenesis of human melanoma xenografts. International Journal of Cancer 1998; 76:836-841.

(37) Pendelton N, Pazouki S, Herkens E, Smither RL, Chisholm DM, Moore JV et al. Relationships between different measurements of vascularity and clinico-pathological parameters in breast cancer. Anticancer Research 1998; 18:4565-4568.

(38) Tomanek R, Scatteman G. Angiogenesis: New insights and therapeutic potential. Anatomical Record 2000; 261:126-135.

(39) Zimmerman M, Selzman CH, Harken AH. Surgical implications of therapeutic angiogenesis. Surgery 1999; 125(3):243-249.

(40) Gleich LL, Zimmerman N, Wang Y-O, Gluckman JL. Angiogenic inhibition for the treatment of head and neck cancer. Anticancer Research 1998; 18:2607-2610.

(41) Ueda N, Kamata N, Hayashi E, Yokoyama K, Hoteiya T, Nagayama M. Effects of an anti-angiogenic agent, TNP-470, on the growth of oral squamous cell carcinomas. Oral Oncology 2000; 35:554-560.

(42) Lingen M. Angiogenesis in the development of head and neck cancer and its inhibition by chemopreventive agents. Critical Reviews of Oral Biology and Medicine 1999; 10(2):153-164.

(43) Smith B, Smith G, Carter D, Sasaki C, Haffty B. Prognostic significance of vascular endothelial growth factor protein levels in oral and oropharyngeal squamous cell carcinoma. Journal of Clinical Oncology 2000; 18:2046-2052.

(44) Williams JK, Carlson GW, Cohen C, Derose PB, Hunter S, Jurkiewicz MJ. Tumor angiogenesis as a prognostic factor in oral cavity tumors. American Journal of Surgery 1999; 168:373-380.

(45) Tahan SR, Stein AL. Angiogenesis in invasive squamous cell carcinoma of the lip : tumor vascularity is not an indicator of metastatic risk. Journal of Cutaneous Pathology 1995; 22:236-240.

(46) Hegde PU, Brenski AC, Caldarelli DD, Hutchinson J, Panje WR, Wood NB et al. Tumor angiogenesis and p53 mutations. Arch Otolaryngol Head Neck 1999; 124:80-85.

(47) Vermeulen P, Gasparini G, Fox S, Toi M, Martin L, McCulloch P et al. Quantification of angiogenesis in solid human tumors: an international consensus on the methodology and criteria of evaluation. European Journal of Cancer 1996; 32A(14):2474-2484.

(48) Folkman J. Clinical applications of research on angiogenesis. New England Journal of Medicine 1995; 26:1757-1763.

(49) Sawa Y, Yoshida S, Ashikaga Y, Kim T, Yamaoka Y, Suzuki M. Immunohistochemical demonstration of lymphatic vessels in human dental pulp. Tissue and Cell 1998; 30(5):510-516.

(50) Miura M, Kato S, von Lüdinghausen M. Lymphatic drainage of the cerebrospinal fluid from monkey spinal meninges with special reference to the distribution of the epidural lymphatics. Archives of Histology and Cytology 1998; 61(3):277-286.

(51) Ebata N, Sawa Y, Ashikaga Y, Yamaoka Y, Suzuki M, Totsuka Y et al. Lymphatic endothelium of the human tongue expresses multiple leukocyte adhesion molecules. Tissue and Cell 1999; 31(1):34-38.

(52) Mukherji SK. Head and neck imaging : the next 10 years. Radiology 1998; 209:8-14.

(53) Haigh P, Giuliano AE. Role of sentinel lymph node dissection in breast cancer. Annals of Medicine 2000; 32:51-56.

(54) Friedman M, Mafee M, Pacella B, Strorigl T, Dew L, Toriumi D. Rationale for elective neck dissection on 1990. Laryngoscope 1990; 100:54-59.

(55) Cabanas R. An approach for the treatment of penile carcinoma. Cancer 1977; 39:626-632.

(56) Krag DN, Weaver EM, Ashikaga T, Moffat FL, Klimberg VS, Shiver C et al. The sentinel node in breast cancer. New England Journal of Medicine 1999; 339(14):941-946.

(57) Ollila D, Brennan M, Guiliano AE. The role of intraoperative lymphatic mapping and sentinel lymphadenectomy in the management of patients with breast cancer. Advances in Surgery 1999; 32:349-364.

(58) McIntosh SA, Purushotham AD. Lymphatic mapping and sentinel node biospy in breast cancer. British Journal of Surgery 1998; 85:1347-1356.

(59) McIntosh SA, Purushotham AD. Lymphatic mapping and sentinel node biopsy in breast cancer. Br J Surg 1998; 85(10):1347-1356.

(60) Statman R, Guiliano AE. The role of the sentinel lymph node in the management of patients with breast cancer. Advances in Surgery 1999; 30:209-221.

(61) Albertini JJ, Lyman GH, Cox C, Yeatment T, Balducci L, Ku N et al. Lymphatic mapping and sentinel node biopsy in the patient with breast cancer. Journal of the American Medical Association 1996; 276(22):1818-1822.

(62) Guiliano AE, Dale PS, Turner RR, Morton DL, Evans SW, Krasne DL. Improved axillary staging of breast cancer with sentinel lymphadenectomy. Annals of Surgery 1995; 222(3):394-401.

(63) Alazraki NP, Eshima D, Eshima LA, Herda SC, Murray DR, Vansant JP et al. Lymphoscintigraphy, the sentinel node concept, and the intraoperative gamma probe in melanoma, breast cancer, and other potential cancers. Seminars in Nuclear Medicine 1997; 27(1):55-67.

(64) Gogel BM, Kuhn JA, Ferry KM, Fisher TL, Preskitt JT, O'Brien JC et al. Sentinel lymph node biopsy for melanoma [In Process Citation]. Am J Surg 1998; 176(6):544-547.

(65) Bostick P, Essner R, Glass E, Kelley M, Sarantou T, Foshag LJ et al. Comparison of blue dye and probe-assisted intraoperative lymphatic mapping in melanoma to identify sentinel nodes in 100 lymphatic basins [In Process Citation]. Arch Surg 1999; 134(1):43-49.

(66) Medl M, Peters-Engl C, Schutz P, Vesely M, Sevelda P. First report of lymphatic mapping with isosulfan blue dye and sentinel node biopsy in cervical cancer. Anticancer Research 2000; 20:1133-1134.

(67) Little AG, DeHoyos A, Kirgan DM, Arcomano TR, Murray KD. Intraoperative lymphatic mapping for non-small cell lung cancer: the sentinel node technique [In Process Citation]. J Thorac Cardiovasc Surg 1999; 117(2):220-224.

(68) Kelemem PR, Van Herle AJ, Guiliano AE. Sentinel lymphadenectomy in thyroid malignant neoplasms. Archives of Surgery 1999; 133:288-292.

(69) Zitsch R, Todd D, Renner G, Singh A. Intraoperative radiolymphoscintigraphy for detection of occult nodal metastasis in patients with head and neck squamous cell carcinoma. Otolaryngology Head and Neck Surgery 2000; 122:662-666.

(70) Alex J, Sasaki C, Krag D, Wenig B, Pyle P. Sentinel lymph node radiolocalization in head and neck squamous cell carcinoma. Laryngoscope 2000; 110:198-203.

(71) Shoaib T, Soutar D, Prosser J, Dunaway D, Gray H, McCurrach G et al. A suggested method for sentinel node biopsy in squamous cell carcinoma of the head and neck. Head & Neck 1999; 21:728-733.

(72) Gennari R, Bartolomei M, Testori A, Zurida S, Stoldt H, Audisio R et al. Sentinel node localization in primary melanoma: preoperative dynamic lymphoscintigraphy, intraoperative gamma probe, and vital dye guidance. Surgery 2000; 126:19-25.

(73) Meyer JS. Sentinel lymph node biopsy: strategies for pathologic examination of the specimen. J Surg Oncol 1998; 69(4):212-218.

(74) Turner RR, Giuliano AE. Intraoperative pathologic examination of the sentinel lymph node [editorial]. Ann Surg Oncol 1998; 5(8):670-672.

(75) Morton D, Ollila D. Critical review of the sentinel node hypothesis. Surgery 1999; 126(5):815-819.

(76) Tonakie A, Sondak V, Yahanda A, Wahl R. Reproducibility of lymphoscintigraphic drainage patterns in sentinel ^{99m}Tc human serum albumin and ^{99m}Tc sulfur colloid studies: implications for sentinel node identification in melanoma. Surgery 2000; 127:955-962.

(77) Olmos R, Jansen L, Hoefnagel C, Muller S, Rutgers E, Kroon B. Evaluation of mammary lymphoscinigraphy by a single intratumoral injection for sentinel node identification. Journal of Nuclear Medicine 2000; 41:1500-1506.

(78) De Cicco C, Cremonesi M, Luini A, Bartolomei M, Grana C, Prisco G et al. Lymphoscintigraphy and radioguided biopsy of the sentinel axillary node in breast cancer. J Nucl Med 1998; 39(12):2080-2084.

(79) Borgstein P, Pijpers R, Comans E, van Diest P, Boom R, Meijer S. Sentinel lymph node biopsy in breast cancer : guidelines and pitfalls of lymphoscintigraphy and gamma probe detection. J Am Coll Surg 1998; 186(3):275-283.

(80) Turner R, Ollila D, Krasne D, Giuliano AE. Histopathologic validation of the sentinel lymph node hypothesis for breast cancer. Annals of Surgery 1997; 226(3):271-278.

(81) Boora R, Bonanni R, Rosato F. Patterns of axillary nodal involvement in breast cancer. Annals of Surgery 1982; 196(6):642-644.

(82) Woolgar J. Detailed topography of cervical lymph node metastases from oral squamous cell carcinoma. Int J Oral Maxillofac Surg 1997; 26:3-9.

(83) Woolgar J, Beirne J, Vaughan E, Lewis-Jones H, Scot J, Brown J. Correlation of histopathologic findings with clinical and radiologic assessments of cervical lymph-node metastases in oral cancer. Int J Oral Maxillofac Surg 1995; 24:30-37.

(84) Stokkel M, ten Broek F, Hordijk G, Koole R, van Rijk P. Preoperative evaluation of patients with primary head and neck cancer using dual-head ^{18}fluorodeoxyglucose positron emission tomography. Annals of Surgery 2000; 231(2):229-234.

(85) Slevin N, Collins C, Hastings D, Waller M, Johnson R, Cowan R et al. The diagnostic value of positron emission tomography (PET) with radiolabeled fluorodeoxyglucose (^{18}F-FDG) in head and neck cancer. Journal of Laryngology and Otology 1999; 113:548-554.

(86) Kau R, Alexiou C, Laubenbacher C, Werner M, Schwaiger M, Arnold W. Lymph node detection of head and neck squamous cell carcinoma by positron emission tomography with fluorodeoxyglucose F18 in a routine clinical setting. Arch Otolaryngol Head Neck 1999; 125:1322-1328.

(87) Dietz A, Delorme S, V, Zuna I, Conradt C. Prognostic assessment of sonography and tumor volumetry in advanced cancer of the heaf and neck y use of Doppler ultrasound. Otolaryngology Head and Neck Srugery 2000; 122:596-601.

(88) Chikui T, Yonetsu K, Nakamura.T. Multivariate feature analysis of sonographic findings of metastatic cervical lymph nodes: contribution of blood flow features revealed by power Doppler sonography for predicting metastasis. AJNR Amercian Journal of Neuroradiology 2000; 21:561-567.

(89) Zurida S, Galimberti V, Orvieto E, Robertson C, Ballardini B, Cremonesi M et al. Radioguided sentinel node biopsy to avoid axillary dissection in breast cancer. Annals of Surgical Oncology 2000; 7(1):28-31.

(90) Proceedings of the Workshop on MR in experimental and clinical cancer research in the new millennium. ISMSM. Geirnanger, Norway, August 2000.

(91) Hirsch JA, Loevner LA, Yousem DM, Siegelman ES, Keiper MD, Marquis RP et al. Gadolinium-enhanced fat-suppressed T1-weighted imaging of the head and neck: comparison of gradient and conventional SE sequences. J Comput Assist Tomogr 1998; 22(5):771-776.

(92) Davis PL, Stainger ML, Harris KB, Ganott MA, Klementaviciene J, McCarthy KS et al. Breast cancer measurements with magnetic resonance imaging, ultrasonography, and mammography. Breast Cancer Research and Treatment 1996; 37:1-9.

(93) Ahrens ET, Rothbächer U, Jacobs RE, Fraser SE. A model for MRI contrast enhancement using T1 agents. Proceedings of the National Academy of Science 1998; 95:8443-8448.

(94) Kelcz F, Santyr GE. Gadolinium-enhanced breast MRI. Critical Reviews in Diagnostic Imaging 1995; 36(4):287-338.

(95) Roberts T. Physiologic measurements by contrast - enhanced MR imaging : expectations and limitations. Journal of Magnetic Resonance Imaging 1997; 7:82-90.

(96) Stubbs M. Application of magnetic resonance techniques for imaging tumor physiology. Acta Oncologica 1999; 38(7):845-853.

(97) Brix G, Bahner ML, Hoffman U, Horvath A, Schreiber W. Regional blood flow, capillary permeability, and compartmental volumes : measurement with dynamic CT - initial experience. Radiology 1999; 210:269-276.

(98) Tofts P. Modeling tracer kinetics in dynamic Gd-DTPA MR imaging. J Magn Reson Imaging 1997; 7(1):91-101.

(99) Kulh CK, Mielcareck P, Klaschik S, Leutner C, Wardelmann E, Gieseke J et al. Dynamic breast MR imaging : are signal intensity time course data useful for differential diagnosis of enhancing lesions? Radiology 1999; 211(1):101-110.

(100) Kelcz F, Santyr GE, Cron GO, Mongin SJ. Application of a quantitative model to differentiate benign from malignant breast lesions detected by dynamic, gadolinium-enhanced MRI. Journal of Magnetic Resonance Imaging 1996; 6:743-752.

(101) Hawighorst H, Knapstein PG, Schaeffer U, Knopp MV, Brix G, Hoffman U et al. Pelvic lesions in patients with treated cervical carcinoma : efficacy of pharmacokinetic analysis of dynamic MR images in distinguishing recurrent tumors from benign conditions. American Journal of Radiology 1996; 166:401-408.

(102) Hawighorst H, Schoenberg SO, Knopp MV, Essig M, Miltner P, van Kaick G. Hepatic lesions : Morphologic and functional characterization with multiphase breath-hold 3D gadolinium enhanced MR angiography - initial results. Radiology 1999; 210:89-96.

(103) Crisci R, DiCesare E, Lupattelli L, Coloni GF. MR study of N2 disease in lung cancer : contrast enhanced method using gadolinium-DPTA. European Journal of Cardio-thoracic Surgery 1997; 11:214-217.

(104) Kusunoki T, Murata K, Hosoi H, Nishida S, Tomura T, Inoue M. Malignancies of human thyroid tumors and dynamic magnetic resonance imaging (MRI) [In Process Citation]. Auris Nasus Larynx 1998; 25(4):419-424.

(105) Tabarin A, Laurent F, Catargi B, Olivier-Puel F, Lescene R, Berge J et al. Comparative evaluation of conventional and dynamic magnetic resonance imaging of the pituitary gland for the diagnosis of Cushing's disease. Clin Endocrinol (Oxf) 1998; 49(3):293-300.

(106) Hawighorst H, Knapstein PG, Weikel W, Knopp MV, Schaeffer U, Brix G et al. Cervical carcinoma : comparison of standard and pharmacokinetic MR imaging. Radiology 1996; 201:531-539.

(107) Hawighorst H, Knapstein PG, Weikel W, Knopp MV, Zuna I, Knof A et al. Angiogenesis of uterine cervical carcinoma : characterization by pharmacokinetic magnetic resonance parameters and histological microvessel density with correlation to lymphatic involvement. Cancer Res 1997; 57:4777-4786.

(108) Buadu LD, Murakami J, Murayama S, Hashiguchi N, Saka S, Toyoshima S et al. Breast lesions: correlation of contrast medium enhancement patterns on MR images with histopathologic findings and tumor angiogenesis. Radiology 1996; 200:639-649.

(109) Mayr NA, Hawighorst H, Yuh W, Essig M, Magnotta V, Knopp MV. MR microcirculation assessment in cervical cancer: correlations with histomorphological tumor markers and clinical outcome. Journal of Magnetic Resonance Imaging 1999; 10:267-276.

(110) Hermans R, Lambin P, der Goten A, den Bogaert W, Verbist B, Weltens C et al. Tumoral perfusion as measured by dynamic computed tomography in head and neck carcinoma. Radiotherapy and Oncology 1999; 53:105-111.

(111) Vaupel P, Hoekel M. Predictive power of the tumor oxygenation status. In: Eke, Delpy, editors. Oxygen Transport to Tissues XXI. New York: Kluwer Academic, 1999: 533-539.

(112) Terris D. Head and neck cancer: The importance of oxygen. Laryngoscope 2000; 110:697-707.

(113) Sundfør K, Lyng H, Rofstad E. Tumor hypoxia and vascular density as predictors of metastasis in squamous cell carcinoma of the uterine cervix. British Journal of Cancer 1998; 78(6):822-827.

(114) Brizel D, Dodge R, Clough R, Dewhirst M. Oxygentation of head and neck cancer: changes during radiotherapy and impact on treatment outcome. Radiotherapy and Oncology 1999; 53:113-117.

(115) Evans S, Hahn S, Pook D, Jenkins W, Chalian A, Zhang P et al. Detection of hypoxia in human squamous cell carcinoma by EF5 binding. Cancer Research 2000; 60:2018-2024.

(116) Raleigh JA, Calkins-Adams DP, Rinker LH, Ballenger CA, Weissler MC, Fowler WC et al. Hypoxia and vascular endothelial growth factor expression in human squamous cell carcinomas using pimonidazole as a hypoxia marker. Cancer Research 1999; 58:3765-3768.

(117) Kalia V, Al-Nabulsi I, Wallen C, Zhang H, Wheeler K. Radiation induced DNA damage in tumors and normal tissues. VI. Estimation of the hypoxic fraction of experimental tumors. Radiation Research 2000; 153:548-556.

(118) Olive P, Horsman M, Grau C, Overgard J. Detection of hypoxic cells in a C3H mouse mammary carcinoma using the comet assay. British Journal of Cancer 1997; 76(6):694-699.

(119) Melo T, Duncan J, Ballinger J, Rauth A. BRU59-21, a second generation ^{99m}Tc-labeled 2-nitroimidazole for imaging hypoxia in tumors. Journal of Nuclear Medicine 2000; 41:169-176.

(120) Moonen C, van Zijl P, Frank J, LeBihan D, Becker E. Functional MRI in medicine and physiology. Science 1990; 4977:53-61.

(121) Li D, Wang Y, Waight DJ. Blood oxygen saturation assessment in vivo using T2* estimation. Magn Reson Med 1998; 39(5):685-690.

(122) Li KC, Wright GA, Pelc LR, Dalman RL, Brittain JH, Wegmueller H et al. Oxygen saturation of blood in the superior mesenteric vein: in vivo verification of MR imaging measurements in a canine model. Work in progress. Radiology 1995; 194(2):321-325.

(123) Chien D, Levin DL, Anderson CM. MR gradient echo imaging of intravascular blood oxygenation: T2* determination in the presence of flow. Magn Reson Med 1994; 32(4):540-545.

(124) Li D, Waight DJ, Wang Y. In vivo correlation between blood T2* and oxygen saturation. J Magn Reson Imaging 1998; 8(6):1236-1239.

(125) Atalay MK, Reeder SB, Zerhouni EA, Forder JR. Blood oxygenation dependence of T1 and T2 in the isolated, perfused rabbit heart at 4.7T. Magn Reson Med 1995; 34(4):623-627.

(126) Wacker C, Bock M, Hartlep A, Bauer W, van Kaick G, Pfleger S et al. BOLD-MRI in ten patients with coronary artery disease: evidence for imaging of capillary recruitment in myocardium supplied by the stenotic artery. Magnetic Resonance Materials in Physics Biology and Medicine 1999; 8:48-54.

(127) Atalay MK, Forder JR, Chacko VP, Kawamoto S, Zerhouni EA. Oxygenation in the rabbit myocardium : assessment with susceptibility dependent MR imaging. Radiology 1993; 189:759-764.

(128) Li D, Oellerich WF, Beck G, Gropler RJ. Assessment of myocardial response to pharmacologic interventions using an improved MR imaging technique to estimate T2 values. AJR Am J Roentgenol 1999; 172(1):141-145.

(129) Prasad P, Edelman R, Epstein F. Noninvasive evaluation of intrarenal oxygenation with BOLD MRI. Circulation 1996; 94(12):3271-3275.

(130) Weissleder R, Elizondo G, Josephson L, Compton CC, Fretz CJ, Stark DD et al. Experimental lymph node metastases : enhanced detection with MR lymphography. Radiology 1989; 171:835-839.

(131) Tanoura T, Bernas M, Darkazanli A, Elam E, Unger E, Witte MH et al. MR lymphography with iron oxide compound AMI-227 : studies in ferrets with filariasis. American Journal of Radiology 1992; 159:875-881.

(132) Taupitz M, Wagner S, Hamm B, Dienemann D, Lawaczeck R, Wolf K-J. MR Lymphography using iron oxide particles : detection of lymph node metastases in the VX2 rabbit tumor model. Acta Radiologica 1999; 34:10-15.

(133) Rogers JM, Jung CW, Lewis J, Growman EV. Use of USPIO induced magnetic susceptibility artifacts to identify sentinel lymph nodes and lymphatic drainage patterns. I. Dependence of artifact size with subcutaneous Combidex dose in rats. Magnetic Resonance Imaging 1998; 16(8):917-923.

(134) Harisinghani M, Saini S, Weissleder R, Hahn P, Yantiss R, Tempany C et al. MR lymphangiography using ultrasmall superparamagnetic iron oxide in patients with primary abdominal and pelvic malignancies : radiologic - pathologic correlation. American Journal of Radiology 1999; 172:1347-1351.

(135) Yamada K, Jinbo T, Miyahara K, Sato M, Hirose T, Kato H et al. Contrast enhanced MRI with gadodiamide injection in rabbit carcinoma models. Journal of Veterinary Medical Sciences 1996; 58(5):389-396.

(136) Belz G, Heath T. Lymphatic drainage from the tonsil of the soft palate in pigs. Journal of Anatomy 1995; 187:491-495.

(137) Hovsepian D, Wu J, Herzog T. Technique for performing direct lymphangiography in pigs. Academic Radiology 1997; 4:361-366.

(138) Jiang D, Gazelle G, Wolf G. A model of focal cancer in rabbit lymph nodes. Academia Radiology 1995; 3:159-162.

(139) Runge V, William N. Investigation of MR contrast media utility with the VX-2 tumor model. Academia Radiology 1998; 5:S34-S36.

(140) Cochran ST, Higashida RT, Holburt E, Winter J, Iwamoto K, Norman A. Development of rabbit brain tumor model for radiologic research. Invest Radiol 1985; 20(9):928-932.

(141) Masåide K, Rofstad EK. Mathematical modeling of chronic hypoxia in tumors considering potential doubling time and hypoxic cell lifetime. Radiotherapy and Oncology 2000; 54:171-174.

(142) Daldrup HE, Shames D, Wendland MF, Okuhata Y, Brasch R, Rosenau W et al. Correlation of dynamic contrast - enhanced MR imaging with histologic tumor grade: comparison of macromolecular and small-molecule contrast media. AJR Am J Roentgenol 1998; 171:941-949.

(143) Kovar D, Lewis M, Karczmar GS. A new method for imaging perfusion and contrast extraction fraction : input functions derived from reference tissues. J Magn Reson Imaging 1998; 8(5):1126-1134.

(144) Nishio H, Tada J, Hashiyama N. CD Guide, Protein Review on the Web. 1997.

(145) Shpitzer T, Chaimoff M, Gal R, Stern Y, Feinmesser R, Segal K. Tumor angiogenesis as a prognostic factor in early oral tongue cancer. Archive of Otolaryngology and Head and Neck Surgery 122, 865-868. 1999.

(146) Penfold CN, Partridge M, Rojas R, Langdon JD. The role of angiogenesis in the spread of oral squamous cell carcinoma. British Journal of Oral and Maxillofacial Surgery 1997; 34:37-41.

(147) Alcalde RE, Terakado N, Otsuki K, Matsumura T. Angiogenesis and expression of platelet-derived endothelial cell growth factor in oral squamous cell carcinoma. Oncology 1997; 54(4):324-328.

(148) Penfold CN, Partridge M, Rojas R, Langdon JD. The role of angiogenesis in the spread of oral squamous cell carcinoma. Br J Oral Maxillofac Surg 1996; 34(1):37-41.

(149) Ross C, Gomaa M, Gillies E, Juengle R, Medina J. Tumor grade, microvessel density, and activities of malate dehydrogenase, lactate dehydrogenase, and hexokinase in squamous cell carcinoma. Otolaryngology Head and Neck Surgery 2000; 122:195-200.

(150) Pazouki S, Chisholm DM, Adi MM, Carmichael G, Farquharson M, Ogden GR et al. The association between tumour progression and vascularity in the oral mucosa. Journal of Pathology 1997; 183:39-43.

(151) Denhart BC, Guidi AJ, Tognazzi K, Dvorak HF, Brown LF. Vascular permiability factor / vascular endothelial growth factor and its receptors in oral and laryngeal squamous cell carcinoma and dysplasia. Laboratory Investigation 1997; 77(6):659-664.

(152) Dellaconon FR, Spiro J, Eisma R, Kreutzer D. Expression of basic fibroblast growth factor and its receptors by head and neck squamous carcinoma tumor and vascular endothelial cells. American Journal of Surgery 1997; 174:540-544.

(153) Witte M, Way D, Witte C, Bernas M. Lymphangiogenesis: mechanisms, significance, and clinical implications. EXS 1997; 79:65-112.

(154) Paavonen K, Puolakkainen P, Jussila L, Jahkola T, Alitalo K. Vascular endothelial growth factor receptor-3 in lymphangiogenesis in wound healing. American Journal of Pathology 2000; 156(5):1499-1504.

(155) Korpelainen E, Alitalc K. Signaling angiogenesis and lymphangiogenesis. Current Opinions in Cel Biology 1998; 10(2):159-164.

(156) Partanen TA, Alitalo K, Miettnen M. Lack of lymphatic vascular specificity of VEGF receptor-3 in 185 vascular tumors. Cancer 1999; 86:2406-2412.

(157) Ohta Y, Shridhar V, Bright R, Kalenkarian G, Du W, Carbone M et al. VEGF and VEGF type play an important role in angiogenesis and lymphangiogenesis in human malignant mesothelioma tumors. British Journal of Cancer 1999; 81(1):54-61.

(158) de Waal RM, van Altena M, Erhard H, Weidle U, Nooijen P, Ruiter D. Lack of lymphangiogenesis in human primary cutaneous melanoma. American Journal of Pathology 1997; 150(6):1951-1957.

(159) Shweiki D, Itin A, Soffer D, Keshet E. Vascular endothelial growth factor induced by hypoxia may mediate hypoxia-initiated angiogenesis. Nature 1992; 359:843-845.

(160) Knopp MV. Personal communication, August 12, 2000.

(161) Brizel D, Sibley G, Prosnitz L, Scher R, Dewhirst M. Tumor hypoxia adversely affects the prognosis of carcinoma of the head and neck. International Journal of Radiation Oncology and Biological Physics 1997; 38(2):285-289.

(162) Thomlinson R, Gray L. The histological structure of some human lung cancers and the possible implications for radiotherapy. British Journal of Cancer 1956; 9(4):539-549.

(163) Swain D, Pittman R. Oxygen exchange in the microcirculation of hamster retractor muscle. American Journal of Physiology 1989; 256(1 pt 2):H247-H255.

(164) Overgaard J, Hansen H, Jorgenson K. Primary radiotherapy of larynx and pharynx carcinoma-an analysis of some factors influencing local control and survival. International Journal of Radiation Oncology and Biological Physics 1986; 12:515-521.

(165) Fein D, Lee, Hanlon A, Ridge J, Langer C, Curran W et al. Pretreatment hemoglobin level influences local control and survival of T1-T2 squamous cell carcinomas of the glottic larynx. Journal of Clinical Oncology 1995; 13(8):2077-2083.

(166) Overgard J. The influence of hemoglobin concentration on the response to radiotherapy. Scandinavian Journal of Clinical Laboratory Investigations 1998; 48:49-53.

(167) Becker A, Stadler P, Lavey R, Hänsgen G, Kuhnt T, Lautenschläger C et al. Severe anemia is associated with poor tumor oxygenation in head and neck squamous cell carcinomas. International Journal of Radiation Oncology and Biological Physics 2000; 46(2):439-466.

(168) Nordsmark M, Overgaard M, Overgaard J. Pretreatment oxygenation predicts radiation response in advanced squamous cell carcinoma of the head and neck. Radiotherapy and Oncology 1996; 41:31-39.

(169) Rudat V, Dietz A, Schramm O, Conradt C, Maier H, Flentje M et al. Prognostic impact of total tumor volume and hemoglobin concentration on the outcome of patients with advanced head and neck cancer after concomitant boost radiochemotherapy. Radiotherapy and Oncology 1999; 53:119-125.

(170) Dietz A, Rudat V, Vanselow B, Wollensack P, Bettscheider C, Conradt C et al. Rise of oxygenation in cervical lymph node metastasis during the initial course of radiochemotherapy. Otolaryngology Head and Neck Surgery 1999; 121:789-796.

(171) Lyng H, Tanum G, Evensen J, Rofstaf E. Changes in oxygen tension during radiotherapy of head and neck tumors. Acta Oncologica 1999; 38(8):1037-1042.

(172) Al-Hallaq HA, River JN, Zamora M, Oikawa H, Karczmar GS. Correlation of magnetic resonance and oxygen microelectrode measurements of carbogen-induced changes in tumor oxygenation. Int J Radiat Oncol Biol Phys 1998; 41(1):151-159.

(173) Al-Hallaq HA, Zamora M, Fish B, Farrell A, Moulder J, Karczmar G. MRI measurements correctly predict the relative effects of tumor oxygenating agents on hypoxic fraction in rodent BA1112 tumors. International Journal of Radiation Oncology and Biological Physics 2000; 47(2):481-488.

(174) Star-Lack J, Adalsteinsson E, Adam M, Terris D, Pinto H, Brown J et al. In vivo 1H MR spectroscopy of human head and neck lymph node metastasis and comparison with oxygen tension measurements. AJNR Amercian Journal of Neuroradiology 2000; 21:183-193.

(175) Teicher B, Lazo J, Sartorelli A. Classification of antineoplastic agents by their selective toxicities toward oxygenated and hypoxic tumor cells. Cancer Research 1981; 41:73-81.

(176) Giatromanolaki A, Koukourakis MI, Georgoulias V, Gatter KC, Harris AL, Fountzilas G. Angiogenesis vs. response after combined chemoradiotherapy of squamous cell head and neck cancer. Int J Cancer 1999; 80(6):810-817.

(177) Bussink J, Kaanders J, Van der Kogel A. Clinical outcome and tumor microenvironmental effects of accelerated radiotherapy with carbogen and nicotinamide. Acta Oncologica 1999; 38(7):875-882.

(178) Bernier J, Denekamp J, Rojas A, Minatel E, Horiot J, Hamers H et al. ARCON: accelerated radiotherapy with carbogen and nicotinamide in head and neck squamous cell carcinomas. The experience of the Co-operative group of radiotherapy of the European organization for research and treatment of cancer (EORTC). Radiother Oncol 2000; 55(2):111-119.

(179) Saunders MI, Hoskin PJ, Pigott K, Powell ME, Goodchild K, Dische S et al. Accelerated radiotherapy, carbogen and nicotinamide (ARCON) in locally advanced head and neck cancer: a feasibility study. Radiother Oncol 1997; 45(2):159-166.

(180) Bellin M, Roy C, Kinkel K, Thoumas D, Zaim S, Vanel D et al. Lymph node metastases : safety and effectiveness of MR imaging with ultrasmall superparamagnetic iron oxide particles - initial clinical experience. Radiology 1998; 207:799-808.

(181) Weissleder R, Stark DD, Engelstad BL, Bacon BR, Compton CC, White DL et al. Superparamagnetic Iron oxide : Pharmacokinetics and Toxicity. American Journal of Radiology 1989; 152:167-173.

(182) Guimaraes R, Clément O, Bittoun J, Carnot F, Frija G. MR lymphography with superparamagnetic iron nanoparticles in rats : pathologic basis for contrast enhancement. American Journal of Radiology 1994; 162:201-207.

(183) Weissleder R, Elizondo G, Wittenberg J, Lee AS, Josephson L, Brady TJ. Ultrasmall superparamagnetic iron oxide : an intravenous contrast agent for assessing lymph nodes with MR imaging. Radiology 1990; 175(2):494-498.

(184) Anzai Y, Blackwell K, Hirschowitz S, Rogers J, Sato Y, Yuh W et al. Initial clinical experience with dextran coated superparamagnetic iron oxide for detection of lymph node metastases in patients with head and neck cancer. Radiology 1994; 192(3):709-715.

(185) Anzai Y, McLachlan S, Morris M, Saxton R, Lufkin RB. Dextran coated superparamagnetic iron oxide, an MR contrast agent for assessing lymph nodes in the head and neck. American Journal of Neuroradiology 1994; 15:87-94.

(186) Anzai Y, Prince MR. Iron oxide enhanced MR lymphography : the evaluation of cervical lymph node metastases in head and neck cancer. Journal of Magnetic Resonance Imaging 1997; 7:75-81.

NOTE TO USERS

The CD-ROM is not included in this original manuscript. It is available for consultation at the author's graduate school library.

This reproduction is the best copy available.